BioChip Journal (2024) 18:22–44
https://doi.org/10.1007/s13206-023-00128-w

REVIEW ARTICLE

Combining Ultrasound-Mediated Intracellular Delivery with Microfluidics in Various Applications

Guangyong Huang[1,2,3] · Lin Lin[1,2,4] · Shixiong Wu[2] · Haojie Dang[2] · Xuesong Cheng[2] · Ying Liu[1,5] · Hui You[1,2,5]

Received: 8 May 2023 / Revised: 11 October 2023 / Accepted: 23 October 2023 / Published online: 28 November 2023

Abstract

Ultrasound-mediated intracellular delivery is one of the popular technologies based on membrane rupture at present. To date, ultrasound directly acts on a large number of cells to achieve cargo delivery and has been widely used in drug delivery, disease therapy and other fields. However, the existing macroscopic methods can no longer meet the requirements of accurate tracking and analysis and are prone to extensive cell damage and even death. With the rapid advancements in microfluidic technologies, the combination of ultrasound and microfluidics (CUM) technology can effectively improve the delivery efficiency and cell survival rates. This new technology has rapidly become a new direction and focus of research. Thus, we analysed the mechanism of sonoporation and the effect of acoustic waves in a microfluidic channel. In addition, we reviewed the application of these new technologies in terms of structure and fabrication of ultrasound transducers and microfluidic devices. As regards our main objective, we hope to help researchers better understand the future developments and the challenges of new technologies. With this review, researchers can promote the development of new technologies to solve the current challenges of intracellular delivery and advance clinical applications.

Keywords Ultrasound · Intracellular delivery · Membrane disruption · Microfluidic · Sonoporation

1 Introduction

Ultrasound, which has the advantages of strong penetration, contactless, mildness and non-invasive operation, can deliver genes, proteins, peptides and other cargoes into cells and has great potential in drug delivery [1–3], disease therapy [4, 5] and other fields. Ultrasound is a method of delivery by physical membrane disruption. Compared to biological and chemical methods, ultrasound minimises or completely avoids the side effects associated with viral vectors [6]. At present, most ultrasound-mediated intracellular delivery adopts ultrasound in a chamber with a certain volume at a macroscopic scale [7–9]. Macroscopic methods, which analyse the average results of a large number of cells, do not meet the requirements of accuracy analysis and single-cell analysis [10, 11]. Considering cavitation microbubbles which have highly random and complex activities at the macroscopic scale, it is impossible to predict when and where the microbubbles will destroy the cell membrane, making in situ microscopic observations of intracellular delivery difficult [12]. At the same time, as the intensity of acoustic fields varies with distance and local overheating, the intensity of the effect on the cells is varied, resulting in damage or death of most cells. The microbubbles produced by ultrasound cavitation have a wide size distribution and random positions, and uncontrollable distances from the cells, all of which directly affect the delivery efficiency [13, 14]. With the advancements in nanotechnology and microfabrication, microfluidic technology is being used increasingly to overcome

✉ Hui You
usmlhy@iim.ac.cn

1 Key Laboratory of Disaster Prevention and Structural Safety of Ministry of Education, Guangxi University, Nanning 530004, China

2 School of Mechanical Engineering, Guangxi University, Nanning 530004, China

3 School of Mechanical and Automotive Engineering, Guangxi University of Science and Technology, Liuzhou 545006, China

4 Guangxi Key Lab of Manufacturing System and Advanced Manufacturing Technology, Nanning 530003, China

5 Guangxi Key Laboratory of Disaster Prevention and Engineering Safety, Guangxi University, Nanning 530004, China

these challenges. Microfluidic technology has the advantages of low sample consumption, simple operation, multifunctional integration, small size and easy portability [15–19]. The microfluidic intracellular delivery platform utilised microchannel with a T-junction cavity structure to induce elongation of recirculating flow, stretching the cells significantly and achieving highly efficient gene delivery into hard-to-transfect primary cells (up to 98%) [20]. To take full advantage of ultrasound technology and microfluidic technology, we need to combine the two technologies and study intracellular delivery at the micrometre scale. Compared with the macroscopic method, microfluidics can be accurately controlled to achieve repairable ultrasound-mediated intracellular delivery at the single-cell level [21]. The combination of ultrasound and microfluidics (CUM) technology to achieve accurate cargo delivery is an important research direction for drug delivery.

The CUM technology acts on the micron-sized channels of the microfluidic chip. It has obvious advantages in delivery efficiency, integration and in situ real-time monitoring. Although the cavitation effect of ultrasound waves is weakened in micro-channels, the microstructure vibrations processed in micro-channels under the action of ultrasound waves can generate acoustic streaming [22]. The cavitation effect causes great damage to cells or even death [23, 24], whilst the mild acoustic streaming method has higher cell viability. The acoustic streaming generated by ultrasound is used in the microchannel to achieve a delivery rate of 65–85%, whilst the cell viability is ≥ 91% [25]. In addition, microfluidics has high-throughput processing capabilities [26] that can deliver up to 1 million cells/min intracellularly on each chip [27]. A high degree of integration in microfluidics allows the simultaneous high-throughput production, purification and characterisation of more than 1500 enzyme variations in a single experiment [28]. Microfluidics can monitor the content changes of cells and other substances in situ in real time, and quantitatively analyse and characterise them [29–31]. Microfluidic are able to combine cell seeding procedure, perfused culture platforms, and subsequent manipulation for cargoes loading inside the cells in the context of ultrasound-mediated intracellular delivery [32].

Applications of the CUM technology in the field of intracellular delivery have developed rapidly; however, these applications have not been surveyed in the past. This article focuses on intracellular delivery in vitro and introduce the application of ultrasound-mediated intracellular delivery combined with microfluidics in detail. In this paper, the mechanism of ultrasound-mediated intracellular delivery, the advantages and applications of the new CUM technology, and future development trends are reviewed. This article focuses on the new theoretical advances derived from the new CUM technology. With this review, we hope to provide a useful reference for the study of ultrasound-mediated intracellular delivery, providing future inspiration for innovative ideas.

2 Microfluidic-Based Sonoporation Method

The most important feature of the CUM technology is that the micro-channels are micron-scale. The main factor that affects fluid behaviour in microchannels is not gravity, but factors, such as diffusion, surface tension and viscosity [33]. Under the same ultrasound field, it has been shown that cavitation events in narrow microchannels are often weaker than those in larger channels [34]. At the same flow rate, the narrow channel has a greater fluid dynamic pressure drop than the large channel, which will also reduce the cavitation effect. Fortunately, researches have shown that microjetting formed by transient cavitation is highly damaging to cells, and microfluidics can just reduce or even avoid the damage to cells caused by transient cavitation. In addition to the common cavitation effect (Fig. 1), the microfluidic-based sonoporation method also includes the acoustic radiation force related to the width of the microchannel and the

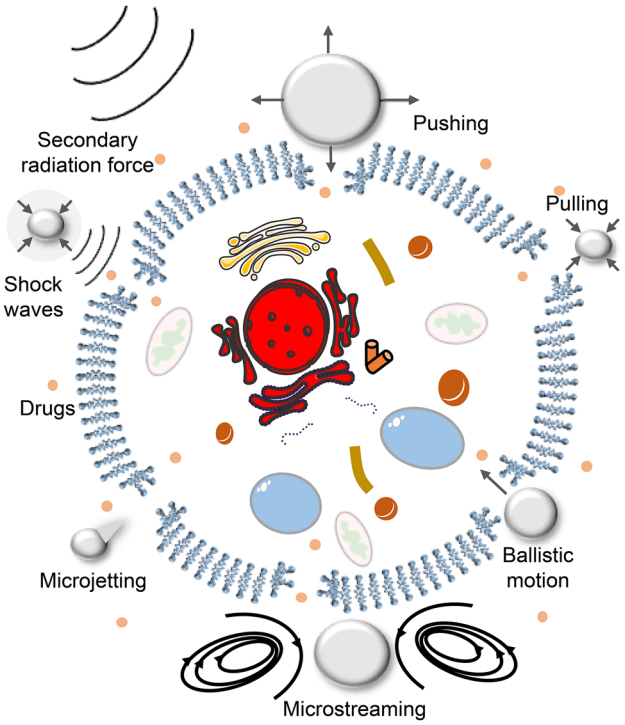

Fig. 1 Schematic diagram of the sonoporation for stable cavitation and transient cavitation. The main forms of ultrasound acting on cells include: pushing, pulling, ballistic motion, microstreaming, microjetting, secondary radiation force, shock waves and acoustic streaming

wavelength, and the acoustic streaming related to the microfluidics (Fig. 2).

2.1 Stable Cavitation and Transient Cavitation

Microfluidic-based sonoporation method has the same cavitation effect as the macroscopic. The propagation of ultrasound waves in the fluid will form alternating pressure changes in space and time. When the acoustic pressure exceeds a certain threshold, the structure of the liquid will be destroyed to form bubbles. The process of alternating growth and contraction of bubbles in a liquid caused by ultrasound is called cavitation, which can be divided into stable cavitation and transient cavitation. The cell is susceptible to the action of adjacent cavitation bubbles, which has a mechanical effect on the cell and alters the membrane permeability (Fig. 1). The central component of the cell membrane is a 5 nm thick phospholipid bilayer with polar heads facing the aqueous environment and fatty acyl chains pointing inward to form a hydrophobic core [35]. After the cell membrane is subjected to stable cavitation and transient cavitation, permeability changes and exogenous substances are delivered into the cell [36]. Stable cavitation is the process of microbubble growth and contraction that cause the surrounding fluid to form microstreaming, pushing or pulling the nearby cell membrane, thus altering their permeability. Transient cavitation is more severe than stable cavitation, and microbubbles eventually collapse to form a microjetting that alters the permeability of the cell membrane. During stable cavitation, the microbubbles alternately grow and contract, and the main effects on cells are pushing, pulling, ballistic motion, microstreaming and secondary radiation force. During transient cavitation, the microbubbles alternately grow, contract and finally collapse, and the effects on the cells include microjettings and shock waves [37–43]. The sonoporation efficiency can be improved to a certain extent by adjusting ultrasound parameters, including acoustic pressure, acoustic energy, isolation time, duty cycle, mechanical index, cavitation index, frequency, pulse duration, time interval after ultrasound exposure, pulse repetition frequency, etc. [44–50].

In addition to the mechanical effects on cells, ultrasound cavitation can also induce chemical, thermal and various biological effects in cells. Researches have shown that reactive oxygen species (ROS) are generated inside cavitation microbubbles [51]. The ROS easily diffuse to the surrounding aqueous phase through the microbubble shell and participate in the permeabilization of nearby cell membrane. The high temperature produced by ultrasound cavitation may affect the physicochemical characteristics of the cell membrane, making it more susceptible to membrane deformation and/or rupture. The relevance of heat effect in the sonopermeabilization of biological barriers remains controversial [52]. Under the action of ultrasound, biological tissues can also cause a variety of biological effects, such as endocytosis and exocytosis. According to studies, cellular uptake is significantly influenced by acoustic pressure, a key factor in determining microbubble activity. Low acoustic pressure increased uptake mostly through promoting endocytosis, whereas high acoustic pressure encourages uptake via the development of membrane pores, termed as sonoporation [10]. Ultrasound not only enhances endocytosis for intracellular delivery but also induces cell exocytosis [53].

2.2 Acoustic Radiation Force

In microchannels, in addition to achieving sonoporation through stable cavitation and transient cavitation, sonoporation can also be assisted by acoustic radiation force. Acoustic radiation force can propel cells to appropriate locations. The cells are subjected to acoustic radiation force and other forces, thereby alter the cell membrane permeability [7, 54,

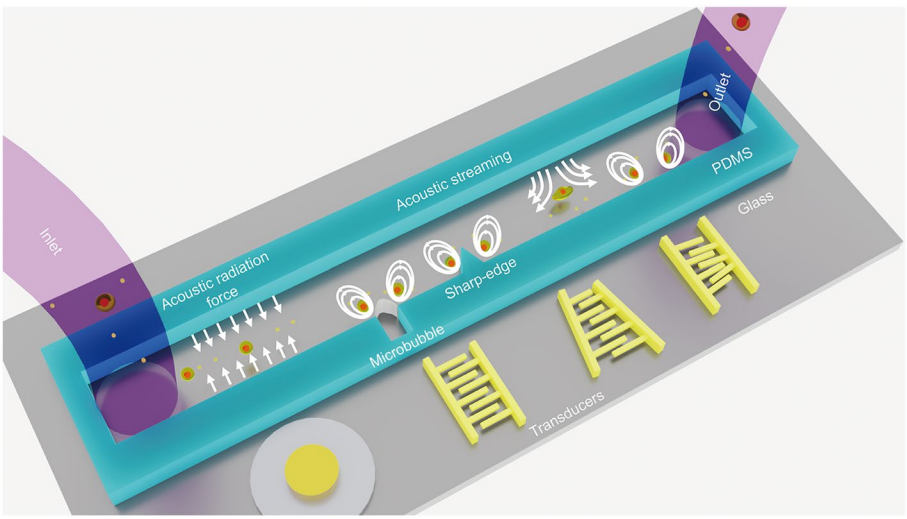

Fig. 2 Schematic diagram of sonoporation by acoustic radiation force and acoustic streaming in microchannels (not to scale). Ultrasound is generated by ultrasound transducers of different structures (e.g. conventional piezoelectric transducer, linear, focussed, slanted or tapered interdigital transducers). Acoustic radiation force moves cells and particles to pressure nodes or antinodes within the microchannel. Acoustic streaming induction methods include microbubbles, sharp-edge structures, adherent cells and pressure waves

55]. Acoustic radiation force method is one of the mild and controlled methods.

When ultrasound waves are applied to the fluid containing the particle suspension in the microchannel, the latter will be affected by acoustic radiation force generated by the scattering of the acoustic waves on the particles. The acoustic radiation force is a crucial parameter in the field of acoustofluidics, where it is most frequently employed for acoustic particle and cell manipulation in microfluidics [56]. Acoustic radiation force is mainly driven by standing waves or surface waves on the fluid [57]. The particular ultrasound with the wavelength close to the height or width of the microchannel can create standing waves inside the microchannel. Particles in standing waves are subjected to acoustic radiation force, which causes them to move to pressure nodes or antinodes (Fig. 2). In theory, particles can be concentrated anywhere in the microchannel as desired. Acoustic radiation forces can propel cells through a constricted nozzle orifice. As cells are ejected from the nozzle, the combination of acoustic radiation force and mechanical force can open pores on the cell membrane [54]. In addition, acoustic radiation force can push cells to the side walls of micro-channels. Cells flow and/or roll along the walls of micro-channels. They experience shear forces induced by microscale acoustic streaming, the acoustic radiation force that pushes the cells to the walls of micro-channels, and forces from the membrane–microchannel wall reaction, resulting in changes in cell permeability [55].

2.3 Acoustic Streaming

Acoustic streaming in micro-channels has the advantages of easy observation, controllability, accuracy, efficiency and mildness. Acoustic streaming can be regarded as any flow generated by the force arising from the presence of a gradient in the time-averaged acoustic momentum flux in a fluid [58]. Therefore, acoustic streaming belongs to the second-order effect, which is different from acoustic radiation force of the first-order effect. This article focuses on microfluidic ultrasound-driven sharp-edge structures or microbubble-induced microstreaming and surface acoustic wave-driven microstreaming. According to the structural characteristics of microfluidics (e.g. microbubbles formed by microcavities and sharp-edge structures formed by processing), various forms of acoustic streaming are formed in microchannels [25, 34, 59–64]. As acoustic streaming does not destroy the structure of the cell membrane, the cells can recover quickly, so the cells have high vitality, even reaching more than 97% [24, 34]. The shear stress induced by the acoustic streaming is used directly in the microchannel to change the permeability of the cell membrane and deliver the exogenous substances to the cells. However, shear stress induced by the acoustic streaming is generally little. Intracellular delivery is the result of a combination with acoustic pressure [24, 60], thermal effects [29] and other factors. Oscillating sharp-edge structures or microstreaming direct current (DC) velocities drop rapidly on viscous boundary layers near microbubbles. If cells happen to be located in this region, the significant shear stress caused by the velocity gradient is the main source of damage to cells. In fact, intracellular delivery results from a combination of frequency, acoustic pressure [24, 60], amplitude, thermal effects [29] and so on.

The most common is the acoustic streaming induced in a fluid by oscillating microbubbles excited by ultrasound in microchannels (Fig. 2). Ultrasound-driven bubble-induced acoustic streaming has been used in cell manipulation and lysis, particle sorting, micromixing and microfluidic pumps [65, 66]. It is particularly pointed out that the microbubbles here are not directly generated by the ultrasound cavitation effect, but are specifically generated by microfluidics. The microbubbles oscillate linearly and non-linearly to form acoustic streaming when driven by ultrasound. Microbubbles produce the strongest acoustic streaming when they oscillate at their resonance frequency. The resonance frequency of the microbubbles is dependent on the microbubble size, its composition and surrounding medium [67]. For a spherical microbubble, Minnaeart's equation can be used to get the resonance frequency. Particularly, the resonant frequency of an air–water bubble at atmospheric pressure and room temperature may be calculated with the help of Eq. (1) [68].

$$f_0 \cong \frac{3.29}{R_b} \tag{1}$$

where f_0 and R_b are the resonant frequency (kHz) and radius (mm) of the microbubble, respectively.

When the microbubble column and the liquid column are formed in the microchannel, the resonant frequency of the microbubble is calculated by the Eq. (2) [69, 70].

$$f_0 = \frac{1}{2}\sqrt{\frac{\kappa P_0}{\rho L_0 L_b}} \tag{2}$$

where P_0 is the pressure of the undisturbed bubble, ρ is the water density, L_0 is the length of the water column, L_b is the length of the microbubble column, and $1 \leq \kappa \leq \gamma$ where γ is the ratio of the specific heats of gas in the bubble.

The active methods generate microbubbles in microchannels based on the types of external fields: acoustic, thermal, electrical, optical, mechanical, magnetic, etc. [68], such as using the T-shaped structure of microchannels to generate microbubbles [74]. The passive methods mainly use the geometry of microfluidics, such as manufacturing by photolithography or micro-milling technologies on the side walls of microchannels can be easily machined to obtain

rectangular cavities and triangular cavities [75–77]. Using triangular cavities in the channel walls, permeable porous barriers and proximal pneumatic channels produce microbubbles with flexible tunability and stability (Fig. 3a) [71]. In addition to designing cavities on the sidewalls of microchannels, it is also to design cavities inside microchannels. Microchannels are designed with various sizes of "horse shoe"-shaped micro-cavity structures to produce microbubbles of various sizes, which are induced by ultrasound to form various acoustic streaming (Fig. 3b) [72]. Microbubbles generated by the array of micro-pores at the bottom of micro-channels form four various and flexibly switchable acoustic streaming driven by various ultrasound frequencies (Fig. 3c) [73].

The sharp-edge structure creates a pair of counter-rotating vortices when oscillating in response to acoustic actuation. Using micromachining technologies, it is easy to achieve sharp-edge structures in microchannels (Fig. 2). The shape of the sharp-edge structure can be triangle, circle and square, and the position of the sharp-edge structure can be located on the left and right sides or the upper and lower sides of the microchannel [78, 79]. An et al. designed a micromechanical oscillator consisting of polygonal-independent plates of variable thickness [80]. The oscillator was sandwiched between two layers of polydimethylsiloxane (PDMS), with the lower layer guiding the fluids to the mixing location and the top layer directing the fluid to the outlet (Fig. 4a, b). When the on-chip piezoelectric transducer was powered by a MHz frequency signal, the sharp inner edge of the vibrating plate created a strong acoustic streaming field (Fig. 4c). The intensity of acoustic streaming formed by the combination of oscillating microbubbles and sharp-edge was higher than that of oscillating microbubbles or sharp-edge alone. Rasouli et al. designed a microfluidic device that incorporates both sharp-edge structure and air microbubbles that could significantly enhance acoustic streaming, thereby increasing the speed and uniformity of mixing (Fig. 4d) [81]. The

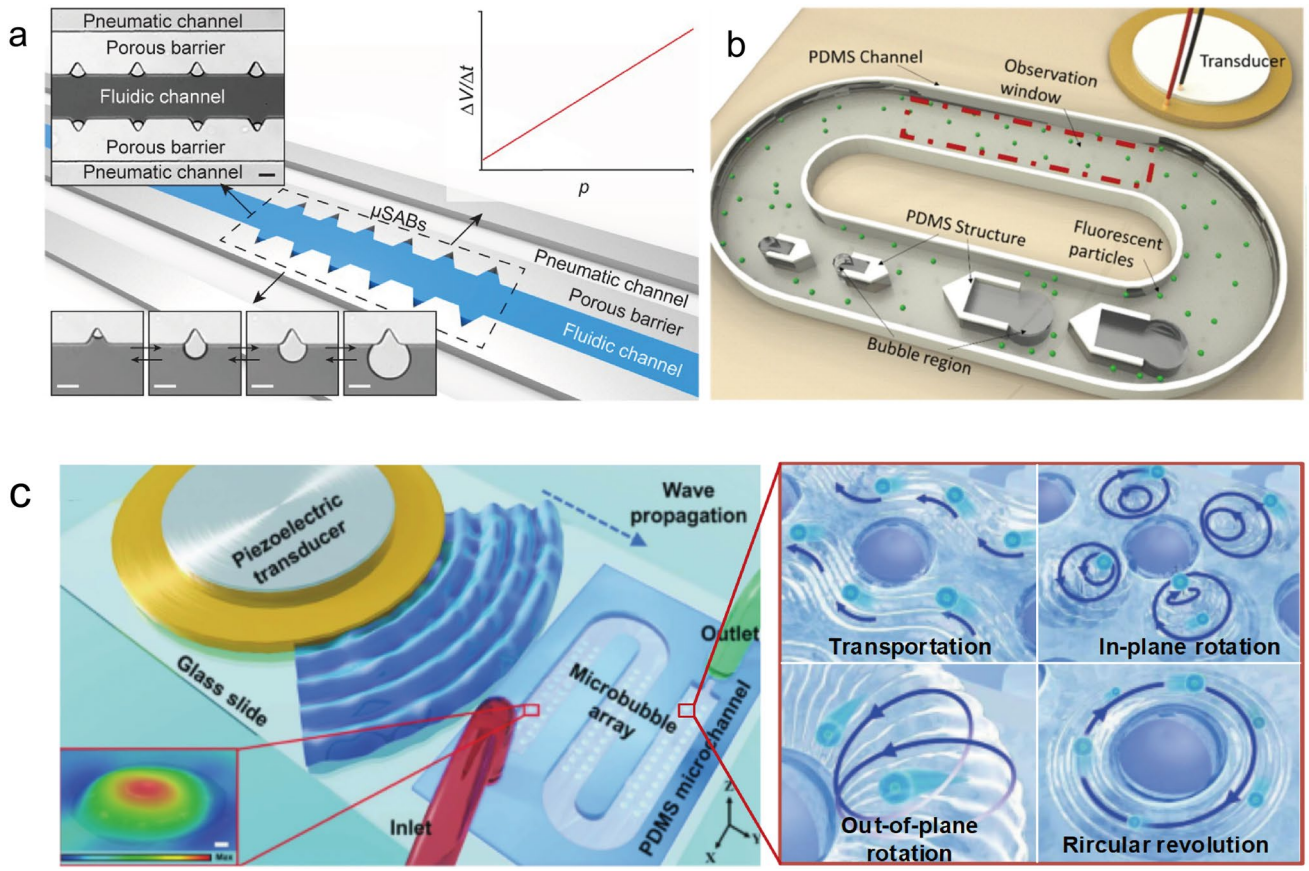

Fig. 3 Microbubble generation and microbubble-induced acoustic streaming in microchannels. **a** A controllable microbubble generation system consisting of triangular cavities in the channel walls, permeable porous barriers and proximal pneumatic channels. Reproduced with permission from Ref. [71]. **b** Various size of "horse-shoe" shaped to produce microbubbles of various sizes. Reproduced with permission from Ref. [72]. **c** Microbubbles are generated by the array of microwells at the bottom of the microchannel. Four acoustic streaming modes of microbubble oscillation (i.e. transportation, in-plane rotation, out-of-plane rotation and circular revolution). Reproduced with permission from Ref. [73]

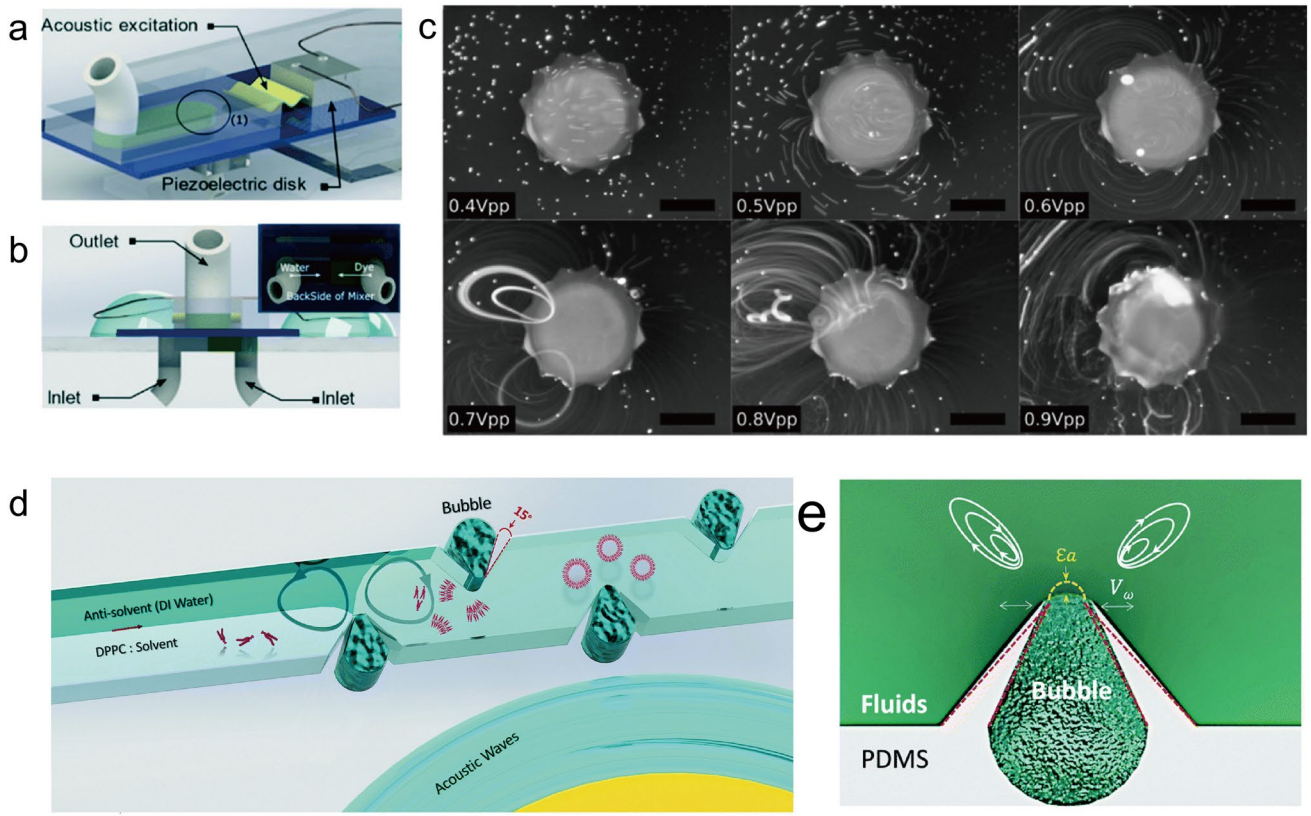

Fig. 4 Acoustic streaming induced by sharp-edge structures in microchannels. **a** Schematic diagram of the micromechanical oscillator device. **b** View of the inlet and outlet from the side. **c** Flow patterns at different driving voltages (the usage of 8 µm particles under fluorescence light). The scale bar is 500 µm. **a**–**c** Reprinted with permission from ref. [80]. **d** Schematic diagram of microbubbles and sharp-edge structure combination. **e** Acoustic streaming induced by sharp-edge and microbubbles. **d**, **e** Reproduced with permission from Ref. [81]

combination of microbubbles and sharp-edge produced stronger acoustic streaming than their simple superposition (Fig. 4e).

Surface acoustic wave (SAW) acts to form pressure waves in the fluid, and acoustic streaming can also be generated by viscous attenuation (Fig. 2). The SAW is generally generated by interdigital transducers (IDTs). IDTs are divided into linear, focussed, slanted or tapered structures according to the layout of the fingers. The IDT design determines the resonant frequency of the SAW device by the finger's geometry. In addition, direction of propagation and bandwidth of the SAW generated are determined by other IDT structural characteristics such as an electrode pair number, electrode shape [83]. Linear structured IDT forms a broader and more homogeneous distribution of acoustic streaming, focussed structure forms a more concentrated, stronger distribution, and slanted or tapered structure forms two counter-rotating vortices. Kamenac et al. designed an interdigital slanted or tapered transducer and a Y-shaped microchannel for the generation of the SAW. The slanted or tapered IDT has a non-uniform finger spacing, where the applied high-frequency signal generates a narrow SAW beam. The narrow SAW beam enters the fluid volume and causes acoustic streaming [84]. The propagation path of the SAW was perpendicular to the microchannel and the two counter-rotating acoustic streamings were generated in the microchannel (Fig. 5a). The two laminar fluids in the Y-shaped microchannel passed through the acoustic streaming region and were uniformly mixed [60].

Recent research has shown that acoustic streaming is also induced when adherent cells attached to microchannels oscillate (Fig. 2). The sharp-edge structures induce acoustic streaming driven by acoustic waves. Therefore, adherent cells attached to the substrate also induce acoustic streaming similar to the substrate raised edge structure. Salari et al. successfully used a specific type of the SAW (i.e. Lamb wave) to drive substrate oscillations to induce microstreaming in adherent cells. The helical streamlines induced around round (Fig. 5b) and flat (Fig. 5c) cells were theoretically and numerically analysed [82].

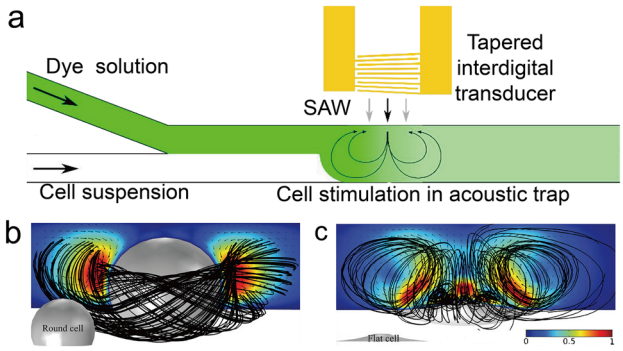

Fig. 5 The SAW and oscillating cells create acoustic streaming in microchannels, respectively. **a** Schematic diagram of the acoustic streaming induced by the SAW. The SAW induced the formation of two vortices that mix the cell suspension (white) and the dye solution (green). Reproduced with permission from Ref. [60]. **b** Numerical simulation of round and flat cells-induced acoustic streaming. Helical-shape streamlines were induced around the two cells. The helical streamlines of the round cell have a greater pitch than those of the flat cell. **b**, **c** Reproduced with permission from Ref. [82]

3 Combined Applications

In view of the many advantages of microfluidic technology, many studies have been carried out on the combination of ultrasound-mediated intracellular delivery and microfluidics. This article describes in detail the applications related to intracellular delivery from both ultrasound transducers and microfluidic devices. The applications show that the combination of ultrasound-mediated intracellular delivery and microfluidics has high delivery rate and high cell viability.

3.1 Ultrasound Transducer

3.1.1 Structural Features

The ultrasound transducer is the key device for generating the sound source in the whole device, which directly affects the effect of intracellular delivery. Ultrasound transducers can be classified by size and geometry. Ultrasound transducers for intracellular delivery in microfluidics can be classified into macroscopic and microscopic according to size, and focussed and non-focussed in terms of geometry. Most ultrasound transducers currently used to study intracellular delivery are macroscopic structures. These researches analyse the average results of large numbers of cells and cannot meet the needs of sophisticated analysis [10, 11].

The micron-scale focussed ultrasound transducer has a small area of action and even targets a single cell. Our group has successfully performed ultrasound gene transfection experiments on a microfluidic chip with a spherical self-focussing Micro-Electro-Mechanical System (MEMS) ultrasound transducer (Fig. 6a, b) [85]. Ultrasound transducers were prepared by sputtering zinc oxide onto polyimide using a magnetron sputtering process to form micron-sized transducers (Fig. 6c). The microfluidic chip for ultrasound gene delivery was obtained by bonding 10 MEMS transducer arrays with PDMS micro-channels (height: 100 μm, width: 200 μm). The simulation analysis showed that the MEMS spherical transducer could form ultrasound cavitation effect in the microchannel, and the ultrasound cavitation effect in the microchannel is verified by the iodine release method. Human renal epithelial cell line (293 T cells) exposed to ultrasound emitted green and red fluorescence after fluorescein diabetic acid (FDA) and propidium iodide (PI) staining, indicating that the cells were successfully perforated by ultrasound and the membrane integrity was repaired (Fig. 6d). Finally, gene introduction experiments were also performed on the biochip and the plasmid was successfully introduced into Hela cells. Thein et al. also used a 3 * 3 transducer array to form an ultrasound micro-transducer array (UMTAs) (Fig. 6e) [86]. The transducers were lead magnesium niobate–lead titanate micro-transducer pillars fabricated into high aspect ratio (height: ~ 120 μm and the cross-sectional area: 25 μm × 25 μm) (Fig. 6f) UMTA was operated by a 30 MHz IDT sinusoidal signal, and the radiation pressure created by ultrasound promotes sonoporation in human melanoma cells (LU1205), with a permeabilization threshold pressure of 0.12 MPa. The biochip technology developed by UMTA has proven cell site-specific sonoporation with excellent spatial specificity and efficient lateral resolution (Fig. 6g). The above experiments demonstrate the potential of micron-scale ultrasound transducers to accurately control and enhance the introduction of substances into cells.

IDTs are often used in microfluidics, and they are designed into different structural forms according to needs. Ramesan et al. performed sonoporation experiments with both straight IDTs and focussing-elliptical single-phase unidirectional transducers (FE-SPUDTs) (Fig. 6h, i) [34, 87]. The IDTs consisted of 127.86° Y–X rotated lithium niobate ($LiNbO_3$) single crystal piezoelectric substrates on which 40 alternating finger pairs of IDTs were photolithographically patterned. High-frequency surface waves could propagate through the fluid coupling layer and the glass bottom of the plate to the fluid domain within the plate. Cells adhered to the glass bottom were exposed to both acoustic radiation force and acoustic streaming-induced shear stress, which led to the reorganisation of lipid structures in the cell membrane. Due to the short duration of action, rapid cell self-healing was observed, leading to high cellular viabilities (> 97%). They exposed Hela cells to high-frequency (> 10 MHz) surface waves for 10 min, and studies revealed that this technology could transport siRNA to cells at a rate of around 40%. Ramesan et al. experimentally found that the acoustic transmission path of the straight IDT was more

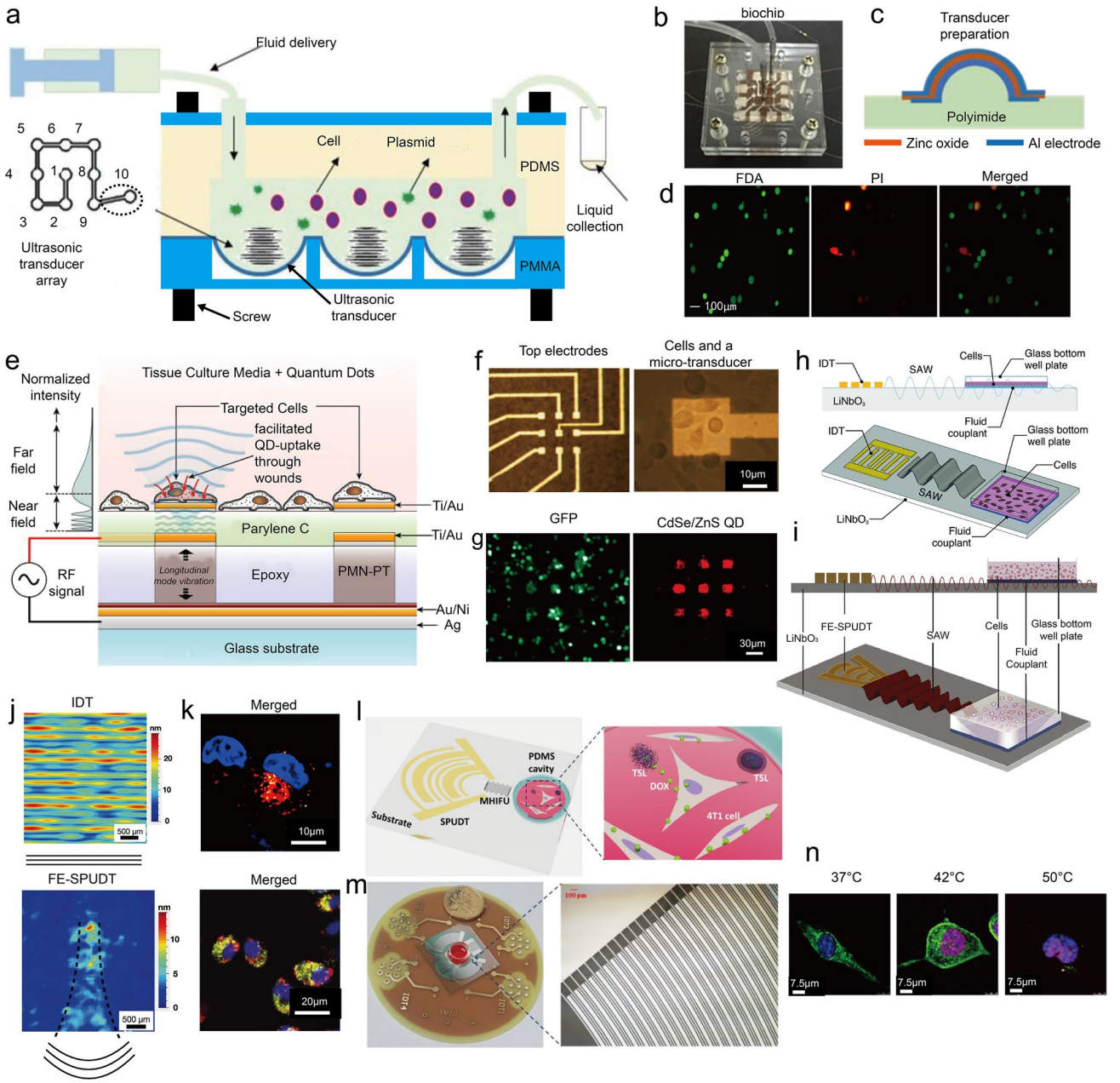

Fig. 6 Ultrasound transducers of different structures for intracellular delivery. **a** Schematic diagram of the MEMS ultrasound transducer microfluidic chip gene transfection experiment. The microchannels are sealed by screws that create a compressive force between the two PMMA surfaces. Due to the large elasticity of PDMS, it deformed under the compression and sealed the microchannel. **b** Microfluidic biochip. **c** Schematic diagram of a self-focussing ultrasound transducer prepared by magnetron sputtering on polyimide. **d** Active cells fluoresce green through FDA (left). PI intracellular DNA binding penetrates the cell membrane of damaged cells and emits red fluorescence (middle). Superimposed Figs (right). **a**–**d** Reproduced with permission from Ref. [85]. **e** Schematic diagram of PMN-PT Microtransducer sonoporation of UMTAs. **f** Brightfield image of the transducer array and the top electrode above (left). LU1205 cells grow above a micro-transducer (right). **g** UMTA-biochip was coated with LU1205 cells expressing GFP (left). LU1205 cells located above the micro-transducers (right). **e**–**g** Reproduced with permission from Ref. [86]. **h** Schematic illustrations of the IDT inside (top) and perspective (bottom) view. **i** Schematic side (top) and perspective (bottom) views of the FE-SPUDT. **j** Using a laser Doppler vibrometer, the root-mean-square surface displacement of the SAW for 10 MHz IDT and 30 MHz FE-SPUDT was determined. **k** The straight IDT and FE-SPUDT of the sonoporation. **h**–**k** Reproduced with permission from Ref. [34, 87]. **l** Schematic diagram of the microscopic high-intensity focussed ultrasound device and microscopic high-intensity focussed ultrasound-mediated temperature-sensitive liposomes release. **m** MHIFU device. **n** The fluorescence image revealed that the drug had penetrated the cellular nuclei following exposure to MHIFU at 42 °C, but nuclear fragmentation and myofilament destruction occurred at 50 °C. **l**–**n** Reproduced with permission from Ref. [29]

broadly distributed, but the FE-SPUDT was more effective at coupling vibrational energy to suspension cells spread throughout the well (Fig. 6j). In contrast to the particle aggregated formed by IDT along the nodal lines of standing waves, it appeared that FE-SPUDT does not produce linear particle aggregates. In the FE-SPUDT platform experiment, when cancer cells were exposed to 30 MHz surface wave for 10 min, the gene knockout efficiency was about 80%, but the cell viability was significantly improved, about 91% (Fig. 6k). The focussed transducer had a high sound intensity due to the focussing effect, and at the same time, the area of action was small, which was more suitable for in situ analysis of single cell. Meng et al. employed miniature high-intensity focussed ultrasound (MHIFU) to thermally trigger drug release to deliver cargoes (Fig. 6l) [29]. A single-phase unidirectional transducer (SPUDT) was fabricated by depositing 40 pairs of circular electrodes on a 1 mm thickness, 128° Y-rotated, X-propagating $LiNbO_3$ substrate to concentrate acoustic energy into a focussed area (Fig. 6m). In the experiment, the solution containing temperature-sensitive liposomes and 4T1 cells was irradiated for 3 min using 30 MHz surface acoustic wave, increasing drug release efficiency. Fluorescence images showed increased cellular uptake with increasing temperature (Fig. 6n). The increase in drug release efficiency was mainly due to the local temperature increase of MHIFU and the mechanical effect caused by acoustic streaming. The biggest feature of the device was the ability to monitor the interaction between cells and ultrasound in situ in real time.

3.1.2 Waveform Types

By reasonably distributing the ultrasound transducer and controlling the drive voltage and signal frequency, different waveforms can be generated and controlled. Different types of ultrasound waveforms can satisfy different intracellular delivery needs. According to the frequency of the acoustic wave, it can be divided into low frequency, medium frequency and high frequency; according to the distribution of the acoustic wave, it can be divided into focussing and non-focussing; according to the relationship between the wavelength of the acoustic wave and the thickness of the substrate, it can be divided into bulk acoustic wave, surface wave and mixed wave [88].

The cells in the microchannel are moved to pressure nodes or antinodes using acoustic radiation force. Adjusting the frequency of the applied acoustic waves relative to the separation between the matching layer and the reflection layer determines the number of pressure nodes and antinodes within the microchannel [89]. Carugo et al. coupled a square piezoelectric transducer (length: 20 mm, width: 6 mm, height: 1 mm) below a glass micro-capillary, and used ultrasound waves in the glass micro-capillary (length: 30 mm, width: 6 mm, inside height: 300 µm, glass thickness: 300 µm) to form standing waves, which could adjust the position of cells and achieved better intracellular delivery (Fig. 7a) [90]. When no contrast agent is present, cardiac myoblasts H9c2 were sonoporated using standing waves to control cell position and the intensity of acoustic radiation. When the capillary reached resonance when the ultrasound frequency was 2.27 MHz, the fluid inside the glass microcapillary would generate a local standing wave. Under the influence of acoustic radiation force, the cells were pushed to the acoustic pressure node on a single focus plane suited for microscope inspection. Ultrasound without contrast media was observed to promote uptake of drugs (apigenin, luteolin and doxorubicin).

Surface wave-based standing wave tweezers are generated using IDT. Four sets of IDTs are utilised to produce two-dimensional pressure nodal fields for cell capture and patterning [89]. Meng et al. designed two pairs of IDTs to distribute around the microbubbles and cells to accurately control the single-cell sonoporation process (Fig. 7b) [21]. The IDT was fabricated by depositing a periodic array of IDTs on the surface of a 128°Y–X $LiNbO_3$ substrate using a standard UV photolithography (Fig. 7c). In both the horizontal and the vertical directions, the finger width and the spacing of the IDTs were 40 µm, which corresponded to a quarter wavelength of the SAW. A microbubble cluster with a diameter of 3.5 µm was delivered to the target cell MCF-7 by relative phases in successive X and Y directions. After the microbubble cluster reached the vicinity of the cell MCF-7, a pulse signal of 24 MHz was applied in the X direction to induce the rupture of the microbubble (Fig. 7d). By accurately controlling the position of the microbubble cluster relative to the target cell, the effective size of collapsed microbubble was measured to be less than 0.68 times the diameter of the microbubble cluster. According to the experimental statistics, the average sonoporation efficiency of the device was $82.4\% \pm 6.5\%$, and the cell viability was $90\% \pm 8.7\%$.

The interaction of ultrasound waves with elastic objects can generate steady-state microstreaming in surrounding liquids. Salari et al. found that the interaction of ultrasound with adherent cells also induced acoustic streaming (Fig. 7e) [82]. At this time, the surface acoustic wave propagated by the ultrasound transducer on the glass substrate was not Rayleigh waves but Lamb waves. Lamb waves were waves where the thickness of the substrate was less than the wavelength of sound. The experimental setup consisted of thin-walled polydimethylsiloxane microchannels and piezoelectric transducers closed to microchannels mounted on a glass substrate. The experiments observed oscillating cell-induced acoustic streaming along with the substrate by monitoring the flow tracer around breast cancer cells MDA-MB-231 (Fig. 7f). The strongest microstreaming was induced by cells

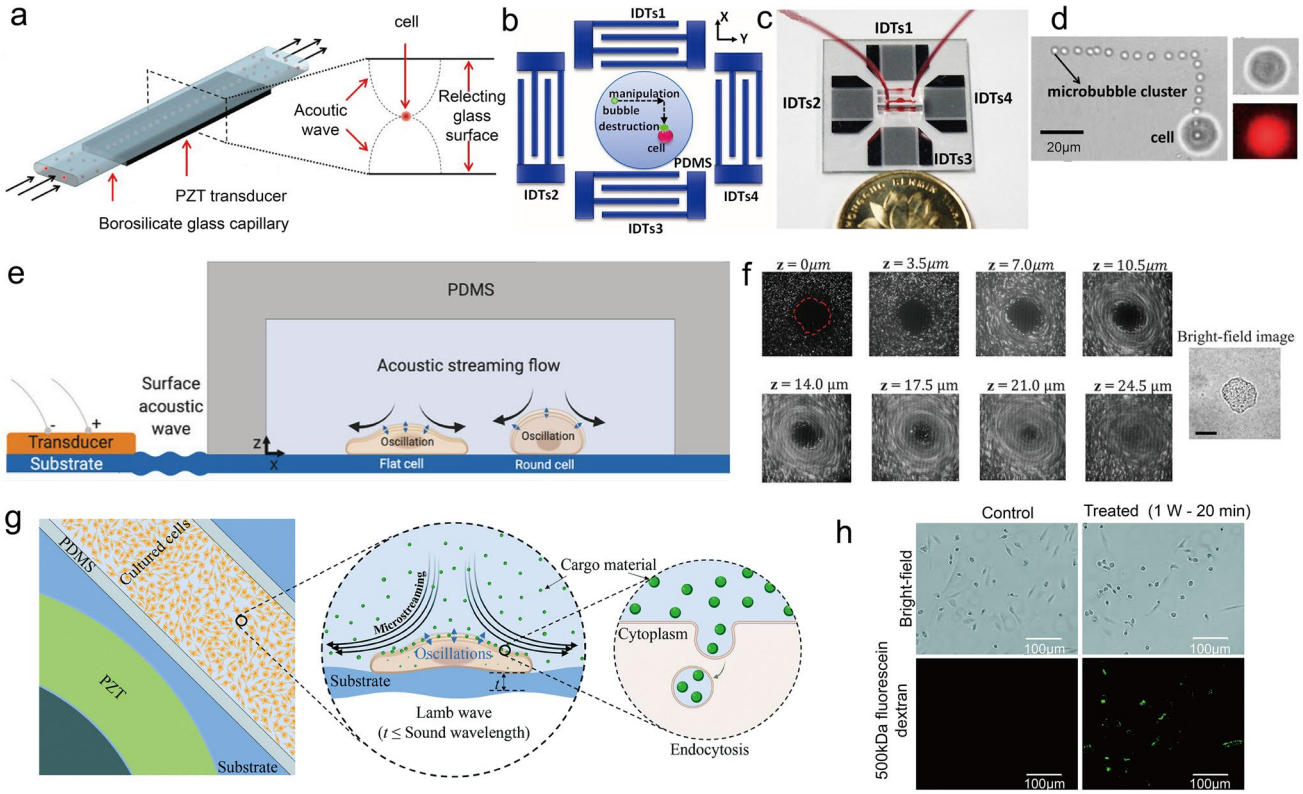

Fig. 7 Intracellular delivery of different waveforms by ultrasound transducers. **a** Using local standing waves to control cell position and sonoporation. Reproduced with permission from Ref. [90]. **b** Schematic diagram of single-cell sonoporation with surface waves distributed around it. **c** Device diagram of single-cell sonoporation. **d** Experiments showed microbubble clusters moving to target cells (left). No obvious changed in cell morphology (upper right). The targeted cell generated red fluorescence (bottom right). **b**–**d** Reproduced with permission from Ref. [21]. **e** Schematic diagram of acoustic streaming generated by the oscillation of adherent cells driven by Lamb wave (not to scale). **f** In the microstreaming of fluorescent particle tracers at different heights from the substrate surface, the heights of maximum microstreaming velocity were 14–21 μm. The MCF-7 cell was shown in bright-field view. **e**, **f** Reproduced with permission from Ref. [82]. **g** Acoustic streaming induced by Lamb wave-driven oscillation of the baseplate and adherent cells promoted cellular uptake of cargoes (not to scale). **h** Bright-field and fluorescence pictures demonstrating the delivery of 500 kDa dextran into MDA-MB-231 cells. **g**, **h** Reproduced with permission from Ref. [25]

at 98 kHz frequency ultrasound drive with velocity up to mm s^{-1}. Subsequently, Salari et al. proposed new acoustically excited in vitro microfluidics for intracellular delivery (Fig. 7g) [25]. Lamb wave-mediated mechanical oscillations in microchannels using ultrasound at a frequency of 96 kHz were used to generate microsteaming near adherent cells. When cells were in microsteaming, they take up cargoes of different sizes through endocytosis, and the cell viability was 91% (Fig. 7h). The experiments successfully delivered dextran molecules of different sizes (3 kDa, 70 kDa and 500 kDa) into PC3, MDA-MB-231 and MCF-7 cells, with an unprecedented 65–85% delivery rate of 500 kDa dextran. The experiments also delivered GAPDH siRNA to MDA-MB-231 cells with a delivery efficiency of about 45%.

Recent researches have shown that hypersonic and sound also have the potential for intracellular delivery. For the first time, Duan et al. used hypersonic to successfully enhance the cellular uptake of different sized drug molecules without the addition of any chemicals [64]. Hypersonic waves have a higher frequency than ultrasound waves, and the acoustic waves attenuate faster and travel shorter distances in viscous fluids, but generate greater liquid driving force. Therefore, the permeability of the cell membrane could be regulated by hypersonic-induced acoustic streaming (Fig. 8a) [91]. As acoustic pressure is proportional to frequency, hypersonic produces greater acoustic pressure than ultrasound and can place greater stress on the cell membrane. Therefore, the use of hypersonic-induced acoustic pressure could also increase the probability of the formation of transient pores in the cell membrane (Fig. 8b) [64]. Duan et al. also successfully applied hypersonic to induce transient nanopores in lipid membrane and vesicles, and successfully performed intracellular delivery of nanomaterials and bioactive substances (e.g. recombinant proteins) [62, 63, 91–93]. Acoustic streaming could also be generated for lower-frequency sound waves [78, 94–96]. The sound transducer drives the

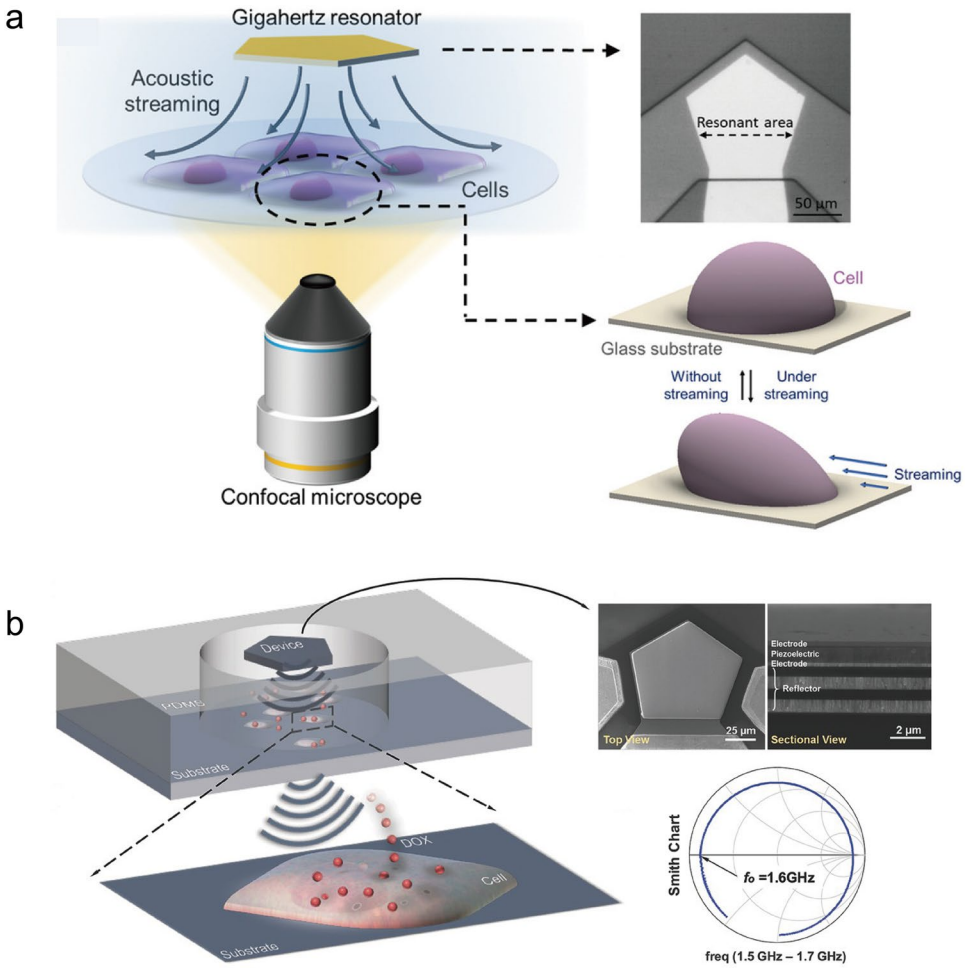

Fig. 8 Intracellular delivery of hypersonic waveforms. **a** Schematic diagram of hypersonic-assisted molecular delivery system using acoustic streaming (left). Optical image of the GHz resonator (top right). Cell deformation under the stimulation of the acoustic streaming (bottom left). Reproduced with permission from Ref. [91]. **b** Schematic diagram of hypersonic-assisted molecular delivery system using acoustic pressure (top left). The top view and the sectional view of the SEM images of the GHz resonator (top right). Cargoes were delivered under hypersonic-induced high-intensity acoustic pressure (bottom left). The smith chart of the resonator device and the resonant frequency is 1.6 GHz (bottom right). Reproduced with permission from Ref. [64]

sharp-edge structure to oscillate to form a microstreaming. The shear stress induced by acoustic streaming is proportional to the microstreaming velocity. Appropriate shear stress is obtained by adjusting the driving voltage of the sound transducer. Song et al. used acoustic streaming generated by oscillating sharp-edge for sonoporation. The device achieved sonoporation at a frequency of 4.6 kHz with a delivery efficiency of over 90% [97]. If the microstreaming is too high, the induced shear stress can damage or even lyse cells [94].

3.2 Microfluidics

3.2.1 Device Structures

The flexible design of the microcavity structure enables the production of microbubbles to control intracellular delivery in microchannels. Microbubbles are produced by ultrasound cavitation or directly pass into the contrast agent [98], whilst microbubbles are randomly distributed in microchannels and the diameters of the microbubbles are different. Microbubbles have no effect on the permeability of the cell membrane when the cells are far away from the microbubbles. As cavitation events are random processes, it is challenging to establish efficient and controllable intracellular delivery of ultrasound. Controlled transient cavitation requires sophisticated equipment, which is costly and inefficient [99, 100]. Stable cavitation can be well regulated in microfluidics. Meng et al. developed a device using a combination of microfluidics and ultrasound that can adjust the membrane permeability in parallel by oscillating microbubble arrays (Fig. 9a) [23]. The microchannels were designed to be multi-rectangular cavities of uniform size on both sides, producing uniform arrays of microbubbles when fluids pass through. Stable harmonic and high harmonic signals were detected in the microchannel under 107 kHz ultrasound exposure, indicating that microbubbles were undergoing stable cavitation. As the effective distance of the microstreaming caused by the oscillation of the microbubble is 3.25 times the diameter of the microbubble [101], the microbubble was able to capture cells within this range. The oscillating microbubble uniform array could realise parallel sonoporation of MDA-MB-231 cells on both sides of the microchannel (Fig. 9b). Experiments showed that when the acoustic pressure was 53.6 kPa

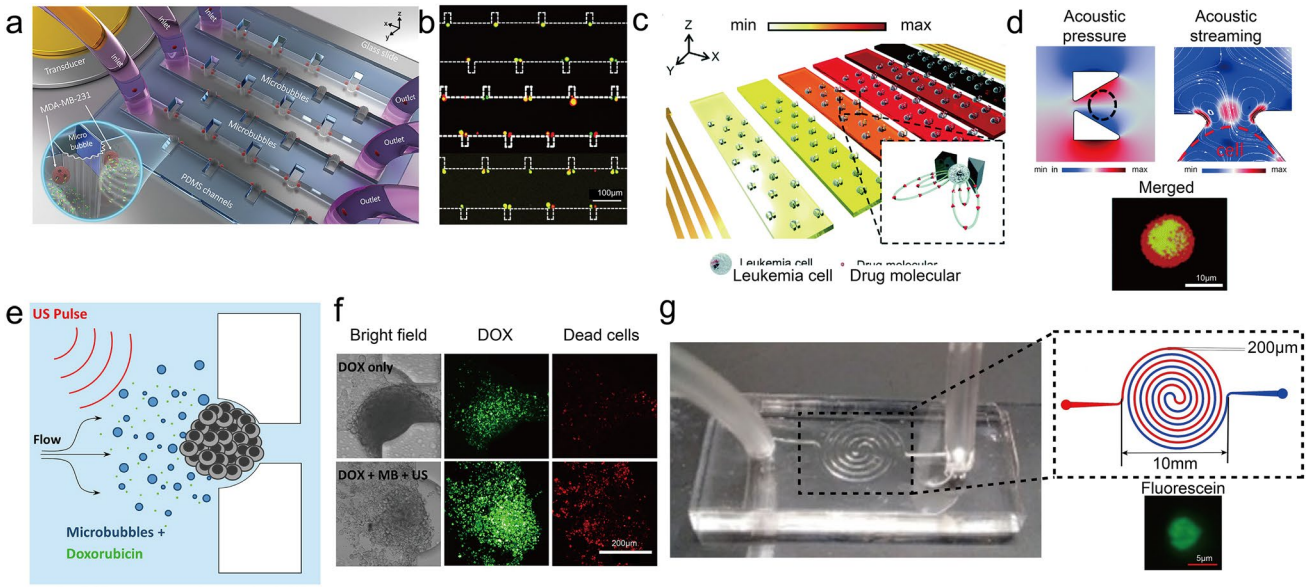

Fig. 9 Microfluidics of different structures for intracellular delivery. **a** Microbubbles were generated in rectangular cavities of the arrays designed on the sidewalls of the micro-channels. Ultrasound-driven microbubbles stabilised cavitation-induced acoustic streaming, trapped nearby cells, and applied shear forces to alter permeability. **b** Under the influence of an oscillating microbubble array, isolated single cells generate a red fluorescence. **a**, **b** Reproduced with permission from Ref. [23]. **c** Design trap structures that capture cells in multiple independent micro-channels, and the acoustic streaming and pressure near cell traps were utilised to accelerate drug uptake by cells. **d** Acoustic pressure simulation near the cell trap (top left). Simulated acoustic streaming field close to the site of the cell trap (top right). Fluorescence picture of a single THP-1 cell treated concurrently with PI and GFP fluorescence following acoustic therapy (bottom). **c**, **d** Reproduced with permission from Ref. [24]. **e** Schematic diagram of the structure of trap structure capturing multiple tumour spheroids. **f** Bright-field, DOX and dead cell (NucRed Dead) fluorescent emission from spheroids 48 h post exposure to DOX only, with MB + US. DOX and dead cell fluorescence brightness. **e**, **f** Reproduced with permission from Ref. [102]. **g** The microchannel structure was a concentric helical delivery device. Microchannel structure dimensions. Fluorescence image of red blood cells (bottom). Reproduced with permission from Ref. [104]

and the treatment time was 90 s, the sonoporation efficiency was 96.6% ± 1.74% and the cell viability was 80.11 ± 1.19%.

Different microstructures can also be designed to accomplish intracellular delivery of different needs in microchannels. Zhao et al. designed a microfluidic chip for single-cell rapid drug screening based on acoustic streaming effect. The microfluidic chip combined high-frequency acoustic waves with concentration gradients and contained 6 independent microchannels, each of which contained a cell trap structure (Fig. 9c) [24]. To induce acoustic streaming, the sharp-edge structures of the trap structures were driven by acoustic waves (> 10 MHz). The tiny shear stress generated by the acoustic streaming disrupted the lipid structure that made up the cell membrane to sufficiently induce transient gaps between lipid molecules. The shear force caused by the acoustic streaming had little damage to the cells, and the cell viability reached 93% after ultrasound exposure. The experiment delivered different concentrations of Ara-C to THP-1 cells to study the effect of different concentrations on the cells. Through shear forces generated by acoustic pressure and acoustic streaming in a non-invasive manner, the cell membrane permeability was gradually altered, and the drug affects cell viability in less than 30 min, faster than conventional methods (> 24 h) (Fig. 9d). Bourn et al. proposed a trap array design on a microfluidic platform for trapping multiple tumour spheroids for drug delivery (Fig. 9e) [102]. To catch the greatest number of tumour spheroids feasible, it was optimised according to the trap array structure designed by Carlo et al. [103]. Each trap was able to capture the flow-through tumour spheroids with a diameter of about 320 μm. Co-delivery of 3 μM doxorubicin (DOX) + microbubbles (MBs) + ultrasound (US) reduced spheroid viability to 48 ± 2%, compared to 75 ± 5% observed with 3 μM DOX alone (Fig. 9f). Therefore, co-administration of MBs + US with DOX has been shown to enhance drug efficacy in both free and liposomal formulations.

Intracellular delivery of different requirements can also be achieved utilising the structural characteristics of microchannels (e.g. the length of microchannels in millimetres). Centner et al. designed a concentric helical microfluidic device in the same area to maximise the length of the microchannel (height: 180 μm, width: 200 μm), thereby exposing the cells to the ultrasound pulse long enough (Fig. 9g) [104]. A solution of red blood cells and microbubbles with an average diameter of 2 ± 1 μm was passed through the microchannel. Red blood cells were exposed to 2.5 MHz

ultrasound and tested by intracellular injection of fluorescein. Changes in ultrasound pressure and mean flow velocity increased fluorescein delivery by 73 ± 37% and 44 ± 33%, respectively. The results showed that this method was a feasible method for the long-term drying of red blood cells at ambient temperature.

3.2.2 Device Material

Microfluidic devices use different materials according to different applications, especially in simulating human microvessels and organs. The most commonly used material is glass micro-capillary. Ankrett et al. utilised square borosilicate glass microcapillaries (length: 50 mm, inner width: 300 µm, wall thickness: 150 µm) as microchannels, which were acoustically coupled to piezoelectric transducers and fixed to glass on the platform. They investigated the effects of ultrasound-related physical parameters, fluid flow rate, temperature, amplitude and frequency on the activity of H9c2 cells (Fig. 10a) [105]. The acoustofluidic device was designed to place an ultrasound transducer on one side of a square glass microcapillary (internal dimensions

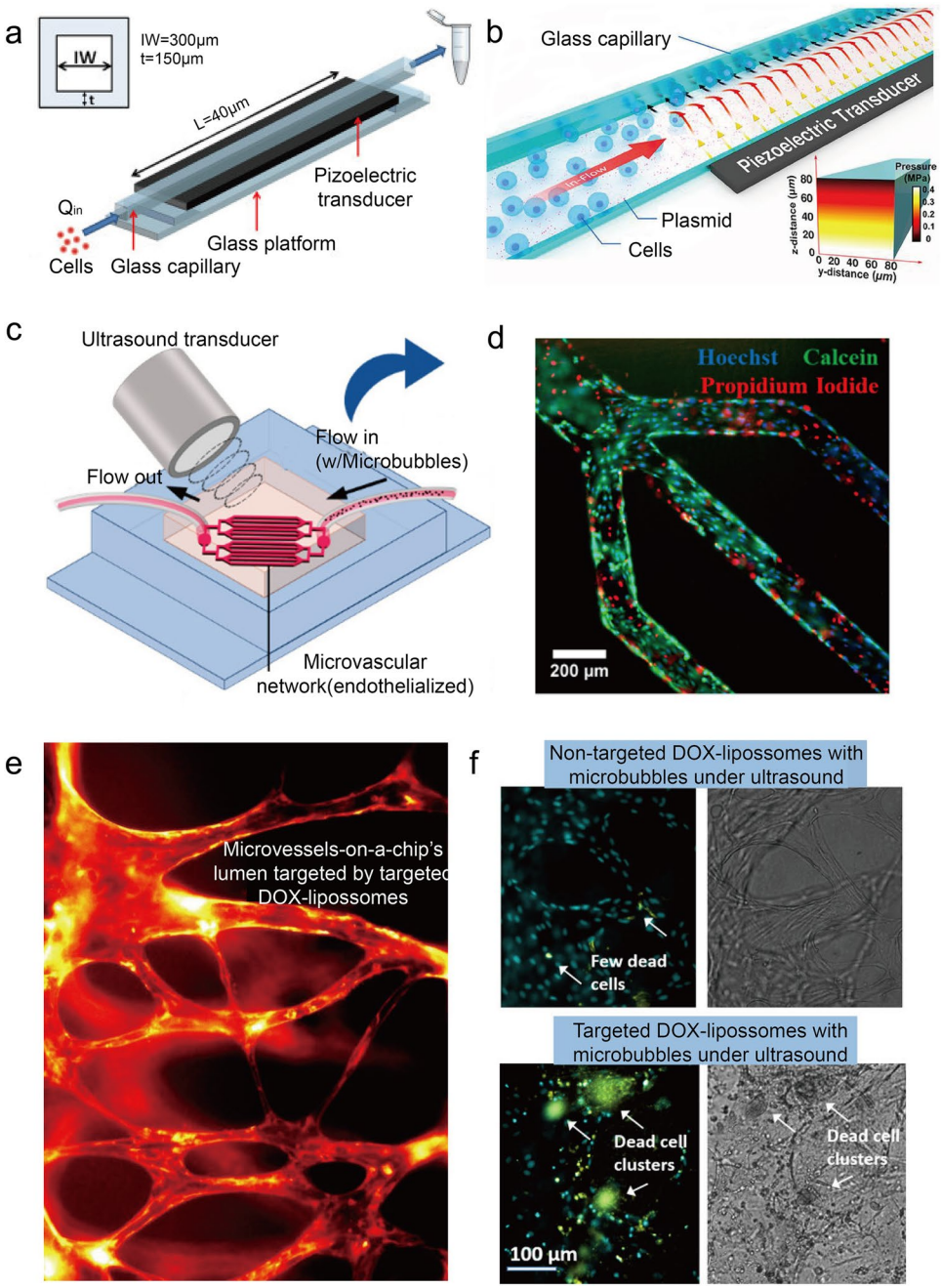

Fig. 10 Intracellular delivery of microfluidic structures of different materials. **a** The device comprising of a squared cross-section glass capillary coupled to the top of the PZT transducer and mounted on a glass platform. Reproduced with permission from Ref. [105]. **b** The device consists of a square-section glass capillary placed on one side of the PZT transducer. Reproduced with permission from Ref. [55]. **c** The in vitro microvascular model is composed of acrylic and PDMS materials, cultured by adding collagen type I solution and collagen I solution. **d** Composite image of Hoechst, DAPI and PI after ultrasound-treated (left). **c**, **d** Reproduced with permission from Ref. [120]. **e** The in vitro microvascular model was prepared with PDMS, and pictures were captured using a TRITC filter after washing to determine DOX fluorescence. **f** In vitro results of the effect of untargeted dox liposomes and integrin-targeted dox liposomes on microbubble ultrasound. **e**, **f** Reproduced with permission from Ref. [121]

of 5 cm × 80 μm × 80 μm) (Fig. 10b) [55]. The ultrasound transducer drove the capillary resonance at a frequency of 3.3 MHz, and the cells were subjected to the shear force caused by the acoustic radiation force and the acoustic streaming, which together change the permeability of the cell membrane. The flowing cells were pushed against the DNA-coated glass capillary walls under the force of acoustic radiation, thereby delivering the DNA into the cells. The device delivered DNA to human hematopoietic stem and progenitor cells in a single channel at a rate of 200,000 cells/min with a viability of over 80%.

Due to its good biocompatibility, PDMS is widely used in in vitro microvascular models that simulate the microenvironment of human blood vessels [106]. Centner et al. delivered trehalose and contrast agent in red blood cells using ultrasound in a PDMS microfluidic chip, significantly increasing the recovery of living red blood cells [104]. Drug delivery in the in vivo models requires intravenous injection through blood vessels, whilst the in vitro models can utilise microfluidics to mimic the vascular microenvironment [107, 108]. In vitro microvascular mimicking vessels are often used for intracellular delivery to reflect realistic in vivo models. Meanwhile, in vivo modelling suffers from the major barriers of high cost and long data collection period, which can be alleviated by microfluidics-based in vitro modelling [109]. Microfluidic-based in vitro models have found applications in various research areas, including the blood–brain barrier, blood–spinal cord barrier, and blood–retinal barrier [39, 110–115]. For instance, the model of the blood–brain barrier on microfluidic chips can be divided into sandwich design, parallel design and 3D tubular structure design [116–118]. The major cells comprising the blood–brain barrier are brain microvascular endothelial cells, which are supported by astrocytes, and pericytes. Endothelial cells have the main features of extremely low rate of transcytosis and forming restrictive paracellular diffusion barriers, which greatly limits the efficiency of substance transport [119]. Consequently, the structural features of the blood–brain barrier impede the delivery of almost all large biomolecules, hindering drug transport to the brain. Over the past decade, efforts have been made to enhance blood–brain barrier permeability using biochemical or physical methods. Amongst drug delivery strategies, ultrasound therapy stands out due to its high efficiency and activity [120, 121]. Currently, microfluidic technology is being employed to create in vitro models of the blood–brain barrier, blood–spinal cord barrier, blood–retinal barrier, etc., to investigate the drug delivery effects of ultrasound and microbubbles on endothelial cells. The development of microfluidic-based in vitro models is poised to play a pivotal role in advancing clinical medicine.

To examine the interaction between microbubbles and vascular endothelium under ultrasound, Juang et al. suggested a perfusable in vitro model with a realistic 3D geometry (Fig. 10c) [120]. The structure of the in vitro microvascular model consisted of 12 channels (each channel length: 7 mm, width: 150 μm, height: 150 μm), which was equivalent to the size of blood vessels. The in vitro microvascular model was composed of acrylic and PDMS materials. A microvascular model with an average diameter of 1.41 μm, seeded with endothelial cells and perfused with cell culture media in vitro. Coupled to the in vitro microvascular network was 1 MHz, single-element, lightly focussed transducer (diameter: 2.01 cm, focal distance: 7.61 cm, focal gain: 2.64). Experiments revealed that increased drug delivery and cell death were both detected with acoustic pressure, with the impact being more prominent at higher pressures (Fig. 10d). Park et al. used in vitro microvascular models to study the effects of drug delivery (Fig. 10e) [121]. Microvascular models were inserted into microbubbles and exposed to ultrasound to analyse the effect of loading non-targeted and targeted doxorubicin-encapsulated liposomes, respectively. With an average microvessel diameter of 39.9 ± 8.58 μm, PDMS microvessel models for hydrogel injection ports and cell culture media reservoirs were fabricated in vitro. A single-element spherically focussed piezoceramic transducer (radius: 63 mm and aperture: 64 mm) was used to generate ultrasound waves at 1.1 MHz and a peak negative pressure of 800 kPa. Dox liposomes (diameter: 78 nm) and microvascular (diameter: 1 μm), which were impermeable to microvascular cells, were introduced into the microvascular. Experiments were performed to compare the effects of cell damage with and without targeted DOX liposomes, microbubbles and ultrasound exposure (Fig. 10f). When targeted doxorubicin-encapsulated liposomes were subjected to low-energy sonication to stabilise micro-vesicle cavitation, cells suffered the most damage, with an average mortality rate of 52 ± 6.7%. In vitro microvascular model flow velocity and ultrasound intensity have an impact on the delivery efficacy, especially blood flow velocity is an important factor in low-intensity ultrasound [122].

PDMS is also used in organ-on-a-chip that simulates human physiological activities [123, 124]. Organ-on-a-chip is a technology that enhances cell function by producing high levels of tissue function in vitro using advanced microfabrication techniques in order to more accurately predict the effects of drugs or other compounds the human body [125–127]. Organ-on-a-chip can manipulate the 3D extracellular environment spatially and temporally by leveraging microfabrication, miniaturisation and controlled engineering technologies [128]. Beekers et al. used an organ-on-a-chip microfluidic platform to study ultrasound intracellular drug delivery [129]. This platform showed the potential to develop in vitro three-dimensional intracellular delivery.

4 Combination with Other Methods

Microfluidics is highly scalable and works well in combination with other technologies. Combining ultrasound with other physical methods in microfluidics can enhance intracellular delivery.

4.1 Applications with Electroporation

Electroporation is a delivery technology that is currently commercialised [130, 131]. Mindaugas et al. investigated various sequential or simultaneous combinations of sonoporation and electroporation on cells in vitro. Experimental studies demonstrated that simultaneous electroporation and sonoporation act on cells to achieve the most efficient intracellular delivery of bleomycin [132]. In addition, they also found the combination of electroporation and sonoporation to enhance the antitumor treatment effect of bleomycin delivery in vivo [133]. In microfluidics, electroporation improves delivery efficiency and cell viability in terms of electrode geometry [134–136] and channel geometry [137–139] variation. Therefore, in the application of microfluidics combining sonoporation and electroporation, the advantages of both can be better played. Longsine-Parker et al. proposed a microfluidic delivery device that achieves high efficiency and high throughput. The device consisted of two parallel 3D electrodes (height: 30 μm, apart: 50 μm) on a glass substrate and a PDMS polymer overlay over the electrodes (Fig. 11a) [140]. Two 3D microelectrodes were placed on both sides

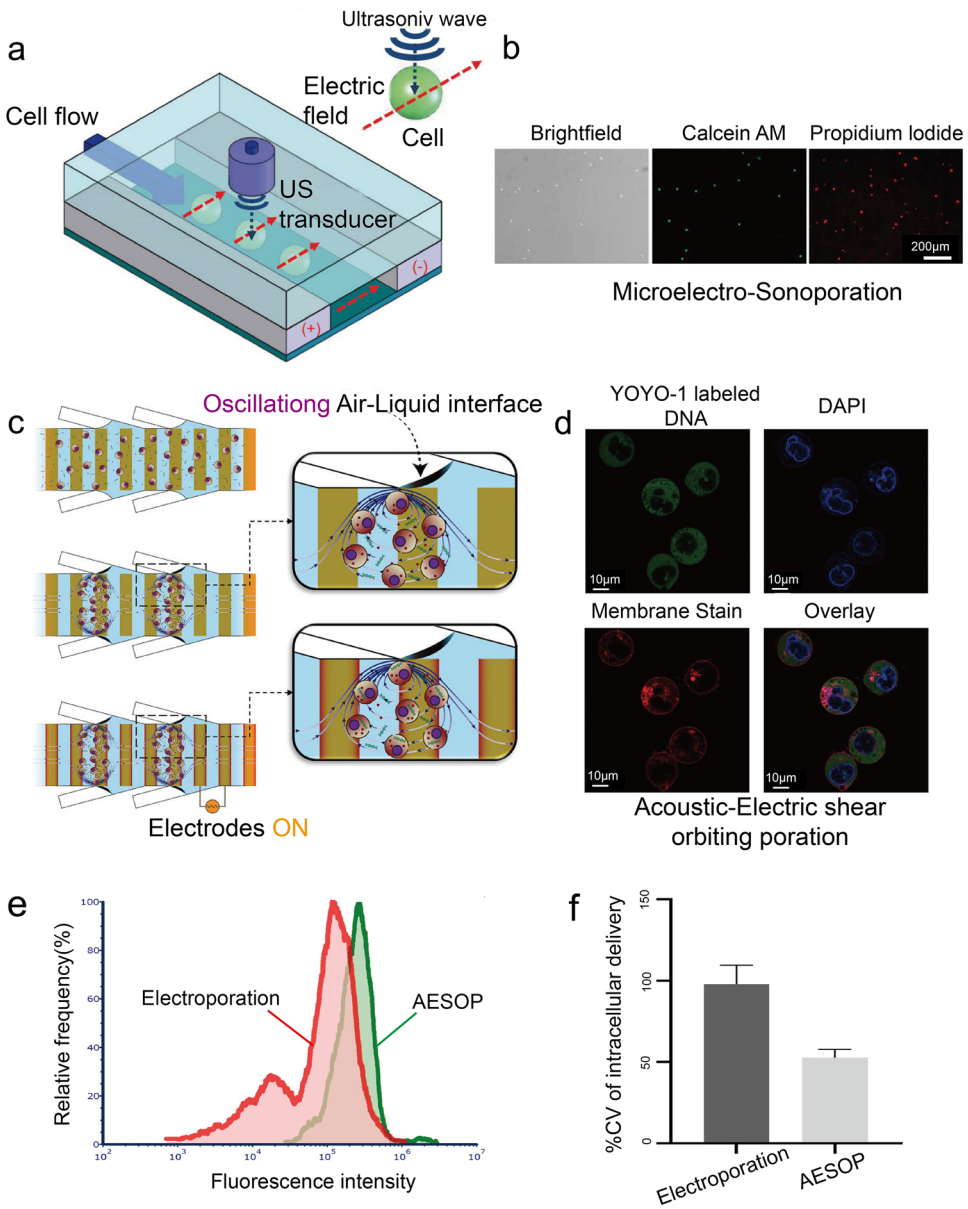

Fig. 11 Cases in combination with other delivery methods. **a** Schematic diagram of the microfluidic electro-acoustic processing device concept. Cells were exposed to electric fields on both sides of the channel and ultrasound at the top as they flow through the microfluidic channel. **b** Brightfield images (left), fluorescence images of live cells stained with Calcein AM (middle), fluorescence images of perforated or non-viable cells stained with PI (right). **a**, **b** Reproduced with permission from Ref. [140]. **c** Schematic diagram of AESOP's operational principle. Cells were subjected to acoustic microfluidic vortices and uniformly exposed to electric fields as they flow through the microfluidic channel. **d** The fluorescence images are in order: YOYO-1 labelled DNA, DAPI, Membrane Stain, Overlay. **e** The histogram of fluorescent intensity of YOYO-1 labelled plasmid DNA delivered into K562 cells using commercial electroporation system and AESOP. **f** The corresponding %CV of intracellular delivery for commercial electroporation system and AESOP. **c**–**f** Reproduced with permission from Ref. [27]

of the PDMS microfluidic channel for electric field generation, and an ultrasound transducer was placed on top of the microfluidic channel. In the experiments, Hela cells were subjected to micro-electroporation and micro-sonoporation at 100 kHz ultrasound and an applied voltage of 8 Vpp. Cells flowed through the microfluidic channel simultaneously under the action of electric field and ultrasound, and the delivery efficiency reached 95.6% (Fig. 11b). The efficiency of micro-electro-sonoporation was 11% higher than sonoporation and 18% higher than micro-electroporation. The cell viability of micro-electro-sonoporation was 97.3%, which was 8% higher than that of micro-electroporation and the same as that of sonoporation. The results showed that the transfection efficiency could be improved by micro-electro-sonoporation, and the level of cell viability was slightly higher or similar to that of the single method.

Aghaamoo et al. also designed a microfluidic platform for intracellular delivery that combines ultrasound-induced acoustic streaming with micro-electroporation, termed Acoustic–Electric Shear Orbiting Poration (AESOP) (Fig. 11c) [27]. The platform consisted of depositing chromium (Cr) and gold (Au) on a glass slide over which PDMS microfluidic channels with sidewall micro-cavities are bonded. First, the cells and the solution flowed into the microfluidic chip, forming microbubbles in the side cavity. Then the piezoelectric transducer under the chip worked, so that the microbubbles in the side cavity oscillated to form acoustic microstreaming vortices. The cells underwent moderate and uniform mechanical shearing in the vortices, thereby creating small pores in the cell membrane. Finally, the pores were uniformly enlarged under the action of the electric field, so that the exogenous large plasmids could enter the cells uniformly and rapidly. The device was capable of delivering various molecular sizes (< 1 kDa to 2 MDa) into adherent and suspension cell lines. From the fluorescence image statistics, the delivery efficiency was > 90%, the cell viability was > 80%, and the throughput processing capacity reached 1 million cells min^{-1}(Fig. 11d). Aghaamoo et al. also compared the performance of AESOP with a commercial electroporation system. According to the results (Fig. 11e, f), AESOP reduces the %CV by half compared to the electroporation. The low %CV achieved by AESOP groups not only confirms delivery of uniform doses across the cell population, but also is an indicator of performance consistency when working with different cargo concentrations.

4.2 Other Delivery Methods

Intracellular delivery with other methods combined with microfluidics has advantages but also faces many challenges. Microinjection uses the advantages of microfluidics for single-cell analysis to perform accurate cell puncture in microfluidics, with higher resolution, lower cost and lower throughput than traditional methods [141–143]. Optoporation uses the laser to accurately locate the focal position to obtain the best position with the cells, but the laser equipment is expensive and has low throughput [100, 144, 145]. In microfluidics cell squeezing technologies, there is use of microchannel geometries to extrude cells and force changes in cell permeability and later use of progressive squeezing to improve delivery efficiency [146–148]. Due to the constant geometry of the constriction, shear stress exerted by the channel walls on cells of different sizes may vary by orders of magnitude, and there is also the problem of easy clogging of the channel [25]. How to combine other delivery methods with ultrasound brings their respective advantages into play.

Applications of ultrasound-mediated intracellular delivery combined with microfluidics are summarised (Table 1). Although some of the articles only studied sonoporation, it has the potential for intracellular delivery and is also categorised as delivery. This paper summarises delivery method, ultrasound frequency, cell type, cargo delivered, delivery efficiency and cell viability. The statistical results of ultrasound frequency, delivery efficiency and cell viability are minimum and maximum of all results for this delivery method. Table 1 demonstrates that acoustic streaming is the delivery technique with the best cell viability. It is important to note that intracellular delivery is a complex process that may be the result of a combination of one or more delivery methods.

5 Current Challenges and Future Perspectives

At present, there are more and more research on the combination of ultrasound-mediated intracellular delivery and microfluidics, and this field has a lot of room for development and potential. With the advancements in technologies in ultrasound and microfluidics, intracellular delivery will play a more important role in biological applications. The future development trend can be summarised as mechanism research, device structure, delivery method and application.

(1) In terms of mechanism, with the new progress of high-speed real-time optical imaging technology, microfluidics can in situ observe and detect the situation of microchannels in real time [152, 153], and even the whole process of delivery [154]. Using boundary element method, Boltzmann and other numerical methods simulate the process of sonoporation. However, the mechanisms of intracellular delivery are not well understood [155]. As the biggest challenge is that there are huge differences in ultrasound cavitation, cargo release and uptake and biological responses on the time scale, and there are huge differences between microbubbles, cells and cargoes on the spatial scale. There

Table 1 Applications of ultrasound-mediated intracellular delivery combined with microfluidics

Delivery method	Ultrasound frequency	Cell type	Cargo delivered	Delivery efficiency	Cell viability	References
Stable cavitation and/or transient cavitation	107 kHz–24 MHz	∗HeLa ∗MCF-7 ∗H9c2 cardiac myoblasts ∗Human umbilical vein endothelial ∗Colorectal cancer (CRC) spheroids ∗Human red blood ∗MDA-MB-231 ∗Human umbilical cord endothelial ∗293 T	∗Doxorubicin ∗Trehalose ∗DOX-Liposomes ∗Dextran (Sigma) ∗Plasmid	16% ± 16–82.4% ± 6.5%	∗– ∗90% ± 8.7% ∗95% ∗– ∗– ∗> 80% ∗96.6% ± 1.74% ∗– ∗–	[21, 23, 85, 98, 102, 104, 105, 120–122, 129, 149, 150]
Acoustic radiation force	2.27 MHz -30 MHz	•H9c2 •Jurkat •PBMC •$CD34^{+}$HSPC •LN443 •Human melanoma (LU1205)	•Doxorubicin •Luteolin •Apigenin •Cy3-DNA	2–62%	•> 70–83% •85% •90% •92% •65–85% •–	[54, 55, 86, 90]
Acoustic streaming	96 kHz–83 MHz	∗HeLa ∗MCF-7 ∗Jurkat ∗THP-1 ∗293 T ∗PC3 ∗MDA-MB-231 ∗YUMM 1.7 ∗Mouse 4T1 breast tumour	∗Temperature-sensitive liposomes ∗Fluorescein dextran ∗Cytarabine (Ara-C) ∗Gold nanoparticles ∗Therapeutic molecules ∗FITC-labelled dextran molecules ∗Glyceraldehyde 3-phosphate dehydrogenase	65–85%	∗> 97% ∗92% ∗> 91% ∗93% ∗> 97% ∗> 91% ∗∗92% ∗–	[24, 25, 29, 34, 60, 87, 151]
Ultrasound and other physical methods	20 kHz–100 kHz	•HeLa •Jurkat •K562	•Plasmid •Dextran	> 80–95.6%	•> 80–97.3% •> 80% •> 80%	[27, 140]

is currently no model to describe the interaction between the three. The CUM technology has significant advantages in contactless delivery, in situ real-time observation, etc., and is a powerful tool to study the mechanism of sonoporation. In the future, it is necessary to integrate multiple disciplines, such as physics, biophysics, biology, chemistry and pharmacology, for research. (2) In terms of devices, microfluidics and ultrasound transducers have rich and flexible designs, diverse structures and sizes ranging from macro to micro, which can meet the needs of different applications. With the advancements in microfabrication technology and lab-on-a-chip technology, the device delivery system is being promoted towards miniaturisation, complexity and large-scale integration. Delivery system devices typically employ PDMS and/or $LiNbO_3$ materials to fabricate microchannels and piezoelectric transducers. These materials are costly and unstable under extreme reaction conditions. Simultaneous fabrication of microchannels and MEMS transducers requires processes, such as photolithography and magnetron sputtering, in a clean room, which is time-consuming and costly to limit the wide adaptability of the device. The application of 3D printing in microfluidics may

solve these problems to some extent [156]. (3) In terms of efficiency, high cell viability and high delivery efficiency are important indicators for evaluating the effectiveness of delivery devices. The delivery method based on microfluidics has achieved good results in specific cells and delivered cargoes, and the efficiency and cell viability are higher than traditional methods. The size variation of exogenous species spans multiple orders of magnitude from nanometres to micrometres. The safe and efficient intracellular delivery of biologically active macromolecules into living cells is a challenging but critical process for research and therapeutic purposes in biotechnology [8, 9, 146, 157, 158]. In addition, the ease of delivery varies by cell types, such as primary cells, progenitor cells and stem cells, which are difficult to transfect. In the future, to solve the problems of flexibility and throughput of the device, it is necessary to make full use of the microfluidic-based sonoporation method to deal with different situations. However, the modes of cavitation, acoustic radiation force and acoustic streaming may exist at the same time, and the primary and secondary relationship of the three in microfluidics and the role of sonoporation are still unclear. At present, the application of ultrasound wave and microfluidics is only combined with electroporation and has not been studied with mechanical, thermal, optical and other physical methods. (4) In terms of applications, intracellular delivery is used in the research of disease mechanism, drug screening, disease treatment, regenerative medicine and other fields. At present, the main research focuses on the basic research of in vitro intracellular delivery, and there is still a certain distance from the delivery application of in vitro cell therapy. With the advancements in 3D bioprinting technology, the future will develop from the current simple models to more complex organ chips applications. Organ chips that simulate the physiological activities of organs have more complex structures [159, 160] and pose higher challenges to ultrasound and microfluidic devices.

6 Conclusions

Over the past few decades, ultrasound as an effective delivery method has shown great potential in bioengineering, biophysics and biomedicine due to its strong penetrability and contactless operation. Microfluidic technology has the advantages of low cost, high throughput and high integration and has been widely used in various fields of biology and medicine. This article reviewed the recent application of the CUM technology in intracellular delivery. Ultrasound mainly acted on cells in the physical way of cavitation effect, acoustic streaming and their combination to cause mechanical, chemical, thermal and biological effects, to achieve the delivery of cargoes into cells from the outside. Combined with microfluidics, it avoided the insufficiency of macroscopic damage to cells, but it weakened the cavitation effect of ultrasound in microchannels. Using microbubbles and sharp-edge in microfluidic microchannels to generate microstreaming enables more efficient delivery and higher cell viability. The applications of intracellular delivery were introduced in detail from the aspects of ultrasound transducer devices and microfluidic devices as well as in combination with other methods. From its rapid advancements, it could be seen that the use of acoustic streaming in microfluidics cell delivery was currently a research hotspot and one of the most effective ways. Finally, we discussed the challenges and directions that ultrasound and microfluidics will face in the future. We believe that the mechanism research of sonoporation will make a breakthrough. In the future, with the advancements in lab-on-a-chip technology, the application of the CUM technology in intracellular delivery will play an important role in solving challenging problems in the biological field.

Acknowledgements This research was funded by the Guangxi Bagui Scholars Project (Grant No. 2019A02), and the Interdisciplinary Scientific Research Foundation of GuangXi University (Grant No. 202200245), and the Guangxi Key Laboratory of Manufacturing System Advanced Manufacturing Technology (Grant No. 15-140-305005), and the Interdisciplinary Scientific Research Foundation of GuangXi University (Grant No. 2022JCB006).

Data availability Data availability is not applicable to this article as no new data were created or analyzed in this study.

Declarations

Conflict of interest The authors declare that they have no conflict of interest.

References

1. Cai, X., Jiang, Y., Lin, M., Zhang, J., Guo, H., Yang, F., Leung, W., Xu, C.: Ultrasound-responsive materials for drug/gene delivery. Front. Pharmacol. **10**, 1650 (2020)
2. Roovers, S., Segers, T., Lajoinie, G., Deprez, J., Versluis, M., De Smedt, S.C., Lentacker, I.: The role of ultrasound-driven microbubble dynamics in drug delivery: from microbubble fundamentals to clinical translation. Langmuir **35**, 10173–10191 (2019)
3. Tharkar, P., Varanasi, R., Wong, W.S.F., Jin, C.T., Chrzanowski, W.: Nano-enhanced drug delivery and therapeutic ultrasound for cancer treatment and beyond. Front. Bioeng. Biotechnol. **7**, 324 (2019)
4. Dimcevski, G., Kotopoulis, S., Bjånes, T., Hoem, D., Schjøtt, J., Gjertsen, B.T., Biermann, M., Molven, A., Sorbye, H., McCormack, E., Postema, M., Gilja, O.H.: A human clinical trial using ultrasound and microbubbles to enhance gemcitabine treatment of inoperable pancreatic cancer. J. Control. Release **243**, 172–181 (2016)
5. Lipsman, N., Meng, Y., Bethune, A.J., Huang, Y., Lam, B., Masellis, M., Herrmann, N., Heyn, C., Aubert, I., Boutet, A., Smith, G.S., Hynynen, K., Black, S.E.: Blood–brain barrier opening in Alzheimer's disease using MR-guided focused ultrasound. Nat. Commun. **9**, 1–8 (2018)
6. Chakrabarty, P., Gupta, P., Illath, K., Kar, S., Nagai, M., Tseng, F., Santra, T.S.: Microfluidic mechanoporation for cellular delivery and analysis. Mater. Today Bio. **13**, 100193 (2022)

7. Rich, J., Tian, Z., Huang, T.J.: Sonoporation: past, present, and future. Adv. Mater. Technol. **7**, 2100885 (2021)
8. Yoon, S., Kim, M.G., Chiu, C.T., Hwang, J.Y., Kim, H.H., Wang, Y., Shung, K.K.: Direct and sustained intracellular delivery of exogenous molecules using acoustic-transfection with high frequency ultrasound. Sci. Rep. **6**, 1–11 (2016)
9. Yoon, S., Wang, P., Peng, Q., Wang, Y., Shung, K.K.: Acoustic-transfection for genomic manipulation of single-cells using high frequency ultrasound. Sci. Rep. **7**, 1–11 (2017)
10. De Cock, I., Zagato, E., Braeckmans, K., Luan, Y., de Jong, N., De Smedt, S.C., Lentacker, I.: Ultrasound and microbubble mediated drug delivery: acoustic pressure as determinant for uptake via membrane pores or endocytosis. J. Control. Release **197**, 20–28 (2015)
11. Tran, D.M., Harrang, J., Song, S., Chen, J., Smith, B.M., Miao, C.H.: Prolonging pulse duration in ultrasound-mediated gene delivery lowers acoustic pressure threshold for efficient gene transfer to cells and small animals. J. Control. Release **279**, 345–354 (2018)
12. Kudo, N.: High-speed in situ observation system for sonoporation of cells with size- and position-controlled microbubbles. IEEE Trans. Ultrason. Ferroelectr. Freq. Control **64**, 273–280 (2017)
13. Qin, P., Xu, L., Han, T., Du, L., Yu, A.C.H.: Effect of non-acoustic parameters on heterogeneous sonoporation mediated by single-pulse ultrasound and microbubbles. Ultrason. Sonochem. **31**, 107–115 (2016)
14. Zhou, Y., Yang, K., Cui, J., Ye, J.Y., Deng, C.X.: Controlled permeation of cell membrane by single bubble acoustic cavitation. J. Control. Release **157**, 103–111 (2012)
15. Schaerli, Y., Wootton, R.C., Robinson, T., Stein, V., Dunsby, C., Neil, M.A.A., French, P.M.W., DeMello, A.J., Abell, C., Hollfelder, F.: Continuous-flow polymerase chain reaction of single-copy DNA in microfluidic microdroplets. Anal. Chem. **81**, 302–306 (2009)
16. Whitesides, G.M.: The origins and the future of microfluidics. Nature **442**, 368–373 (2006)
17. Han, J., Kang, U., Moon, E., Yoo, H., Gweon, B.: Imaging technologies for microfluidic biochips. BioChip J. **16**, 255–269 (2022)
18. Kim, J., Kim, S., Uddin, S., Lee, S.S., Park, S.: Microfabricated stretching devices for studying the effects of tensile stress on cells and tissues. BioChip J. **16**, 366–375 (2022)
19. Kim, T., Jo, K.: Microfluidic device to maximize capillary force driven flows for quantitative single-molecule DNA analysis. BioChip J. **17**, 384–392 (2023)
20. Hur, J., Park, I., Lim, K.M., Doh, J., Cho, S., Chung, A.J.: Microfluidic cell stretching for highly effective gene delivery into hard-to-transfect primary cells. ACS Nano **14**, 15094–15106 (2020)
21. Meng, L., Cai, F., Jiang, P., Deng, Z., Li, F., Niu, L., Chen, Y., Wu, J., Zheng, H.: On-chip targeted single cell sonoporation with microbubble destruction excited by surface acoustic waves. Appl. Phys. Lett. **104**, 73701 (2014)
22. Muller, P.B., Barnkob, R., Jensen, M.J.H., Bruus, H.: A numerical study of microparticle acoustophoresis driven by acoustic radiation forces and streaming-induced drag forces. Lab Chip **12**, 4617–4627 (2012)
23. Meng, L., Liu, X., Wang, Y., Zhang, W., Zhou, W., Cai, F., Li, F., Wu, J., Xu, L., Niu, L., Zheng, H.: Sonoporation of cells by a parallel stable cavitation microbubble array. Adv. Sci. **6**, 1900557 (2019)
24. Zhao, S., Hu, X., Zhu, J., Luo, Z., Liang, L., Yang, D., Chen, Y., Chen, L., Zheng, Y., Qinghao, H., Zheng, J., Guo, S., Cheng, Y., Zhou, F., Yang, Y.: On-chip rapid drug screening of leukemia cells by acoustic streaming. Lab Chip **21**, 4005–4015 (2021)
25. Salari, A., Appak-Baskoy, S., Coe, I.R., Abousawan, J., Antonescu, C.N., Tsai, S.S.H., Kolios, M.C.: Dosage-controlled intracellular delivery mediated by acoustofluidics for lab on a chip applications. Lab Chip **21**, 1788–1797 (2021)
26. Hu, X., Zhao, S., Luo, Z., Zuo, Y., Wang, F., Zhu, J., Chen, L., Yang, D., Zheng, Y., Zheng, Y., Cheng, Y., Zhou, F., Yang, Y.: On-chip hydrogel arrays individually encapsulating acoustic formed multicellular aggregates for high throughput drug testing. Lab Chip **20**, 2228–2236 (2020)
27. Aghaamoo, M., Chen, Y.H., Li, X., Garg, N., Jiang, R., Yun, J.T.H., Lee, A.P.: High-throughput and dosage-controlled intracellular delivery of large cargos by an acoustic-electric microvortices platform. Adv. Sci. **9**, 2102021 (2022)
28. Markin, C.J., Mokhtari, D.A., Sunden, F., Appel, M.J., Akiva, E., Longwell, S.A., Sabatti, C., Herschlag, D., Fordyce, P.M.: Revealing enzyme functional architecture via high-throughput microfluidic enzyme kinetics. Science **373**, eabf8761 (2021)
29. Meng, L., Deng, Z., Niu, L., Li, F., Yan, F., Wu, J., Cai, F., Zheng, H.: A disposable microfluidic device for controlled drug release from thermal-sensitive liposomes by high intensity focused ultrasound. Theranostics. **5**, 1203–1213 (2015)
30. Su, E.J., Herr, A.E.: Electrophoretic cytometry of adherent cells. Lab Chip **17**, 4312–4323 (2017)
31. Namli, I., Karavelioglu, Z., Sarraf, S.S., Aghdam, A.S., Varol, R., Yilmaz, A., Sahin, S.B., Ozogul, B., Bozkaya, D.N., Acar, H.F., Uvet, H., Çetinel, S., Kutlu, Ö., Ghorbani, M., Koşar, A.: On the application of hydrodynamic cavitation on a chip in cellular injury and drug delivery. Lab Chip **23**, 2640–2653 (2023)
32. Morshedi, R.D., Alsadat, R.M., Razavi, B.S., Kashaninejad, N., Jin, D., Ebrahimi, W.M.: A comprehensive review on intracellular delivery. Adv. Mater. **33**, e2005363 (2021)
33. Zhao, Q., Cui, H., Wang, Y., Du, X.: Microfluidic platforms toward rational material fabrication for biomedical applications. Small **16**, 1903798 (2019)
34. Ramesan, S., Rezk, A.R., Dekiwadia, C., Cortez-Jugo, C., Yeo, L.Y.: Acoustically-mediated intracellular delivery. Nanoscale **10**, 13165–13178 (2018)
35. Stewart, M.P., Langer, R., Jensen, K.F.: Intracellular delivery by membrane disruption: mechanisms, strategies, and concepts. Chem. Rev. **118**, 7409–7531 (2018)
36. Fechheimer, M., Boylan, J.F., Parker, S., Sisken, J.E., Patel, G.L., Zimmer, S.G.: Transfection of mammalian cells with plasmid DNA by scrape loading and sonication loading. Proc. Natl. Acad. Sci. PNAS. **84**, 8463–8467 (1987)
37. Bader, K.B., Gruber, M.J., Holland, C.K.: Shaken and stirred: mechanisms of ultrasound-enhanced thrombolysis. Ultrasound Med. Biol. **41**, 187–196 (2015)
38. Chen, H., Brayman, A.A., Kreider, W., Bailey, M.R., Matula, T.J.: Observations of translation and jetting of ultrasound-activated microbubbles in mesenteric microvessels. Ultrasound Med. Biol. **37**, 2139–2148 (2011)
39. Kooiman, K., Roovers, S., Langeveld, S.A.G., Kleven, R.T., Dewitte, H., O'Reilly, M.A., Escoffre, J., Bouakaz, A., Verweij, M.D., Hynynen, K., Lentacker, I., Stride, E., Holland, C.K.: Ultrasound-responsive cavitation nuclei for therapy and drug delivery. Ultrasound Med. Biol. **46**, 1296–1325 (2020)
40. Kudo, N., Kinoshita, Y.: Effects of cell culture scaffold stiffness on cell membrane damage induced by sonoporation. J. Med. Ultrason. **41**, 411–420 (2014)
41. Pereno, V.: Characterisation of Microbubble-Membrane Interactions in Ultrasound Mediated Drug Delivery. University of Oxford, Oxford (2018)
42. Suzuki, R., Oda, Y., Utoguchi, N., Maruyama, K.: Progress in the development of ultrasound-mediated gene delivery systems utilizing nano- and microbubbles. J. Control. Release **149**, 36–41 (2011)
43. van Wamel, A., Kooiman, K., Harteveld, M., Emmer, M., Ten Cate, F.J., Versluis, M., de Jong, N.: Vibrating microbubbles

poking individual cells: drug transfer into cells via sonoporation. J. Control. Release **112**, 149–155 (2006)
44. Cancelos, S., Moraga, F.J., Lahey, R.T., Shain, W., Parsons, R.H.: The effect of acoustically-induced cavitation on the permeance of a bullfrog urinary bladder. J. Acoust. Soc. Am. **128**, 2726–2738 (2010)
45. Escoffre, J., Novell, A., Piron, J., Zeghimi, A., Doinikov, A., Bouakaz, A.: Microbubble attenuation and destruction: are they involved in sonoporation efficiency? IEEE Trans. Ultrason. Ferroelectr. Freq. Control **60**, 46–52 (2012)
46. Forbes, M.M., Steinberg, R.L., O'Brien, W.J.: Frequency-dependent evaluation of the role of definity in producing sonoporation of Chinese hamster ovary cells. J. Ultrasound. Med. **30**, 61–69 (2011)
47. Huang, T.Y.Y.C.K.: Dual-frequency excitation enhances targeted delivery of ultrasound microbubbles. In: Ultrasonics Symposium, vol. 1956–1959. IEEE (2010)
48. Karshafian, R., Bevan, P.D., Williams, R., Samac, S., Burns, P.N.: Sonoporation by ultrasound-activated microbubble contrast agents: effect of acoustic exposure parameters on cell membrane permeability and cell viability. Ultrasound Med. Biol. **35**, 847–860 (2009)
49. Qiu, Y., Zhang, C., Tu, J., Zhang, D.: Microbubble-induced sonoporation involved in ultrasound-mediated DNA transfection in vitro at low acoustic pressures. J. Biomech. **45**, 1339–1345 (2012)
50. Shapiro, G., Wong, A.W., Bez, M., Yang, F., Tam, S., Even, L., Sheyn, D., Ben-David, S., Tawackoli, W., Pelled, G., Ferrara, K.W., Gazit, D.: Multiparameter evaluation of in vivo gene delivery using ultrasound-guided, microbubble-enhanced sonoporation. J. Control. Release **223**, 157–164 (2016)
51. Escoffre, J., Campomanes, P., Tarek, M., Bouakaz, A.: New insights on the role of ROS in the mechanisms of sonoporation-mediated gene delivery. Ultrason. Sonochem. **64**, 104998 (2020)
52. Lentacker, I., De Cock, I., Deckers, R., De Smedt, S.C., Moonen, C.T.W.: Understanding ultrasound induced sonoporation: definitions and underlying mechanisms. Adv. Drug Deliv. Rev. **72**, 49–64 (2014)
53. Yuana, Y., Jiang, L., Lammertink, B., Vader, P., Deckers, R., Bos, C., Schiffelers, R., Moonen, C.: Microbubbles-assisted ultrasound triggers the release of extracellular vesicles. Int. J. Mol. Sci. **18**, 1610 (2017)
54. Zarnitsyn, V.G., Meacham, J.M., Varady, M.J., Hao, C., Degertekin, F.L., Fedorov, A.G.: Electrosonic ejector microarray for drug and gene delivery. Biomed. Microdevice **10**, 299–308 (2008)
55. Belling, J.N., Heidenreich, L.K., Tian, Z., Mendoza, A.M., Chiou, T.-T., Gong, Y., Chen, N.Y., Young, T.D., Wattanatorn, N., Park, J.H., Scarabelli, L., Chiang, N., Takahashi, J., Young, S.G., Stieg, A.Z., De Oliveira, S., Huang, T.J., Weiss, P.S., Jonas, S.J.: Acoustofluidic sonoporation for gene delivery to human hematopoietic stem and progenitor cells. Proc. Natl. Acad. Sci. U. S. A. **117**, 10976–10982 (2020)
56. Bruus, H.: Acoustofluidics 7: the acoustic radiation force on small particles. Lab Chip **12**, 114–121 (2012)
57. Chen, Y., Fang, Z., Merritt, B., Strack, D., Xu, J., Lee, S.: Onset of particle trapping and release via acoustic bubbles. Lab Chip **16**, 324–332 (2016)
58. Wiklund, M., Green, R., Ohlin, M.: Acoustofluidics 14: applications of acoustic streaming in microfluidic devices. Lab Chip **12**, 2438–2451 (2012)
59. Doinikov, A.A., Thibault, P., Marmottant, P.: Acoustic streaming induced by two orthogonal ultrasound standing waves in a microfluidic channel. Ultrasonics **87**, 7–19 (2018)
60. Kamenac, A., Schilberth, F.L., Wagner, E., Wixforth, A., Lächelt, U., Westerhausen, C.: Transient permeabilization of living cells: combining shear flow and acoustofluidic trapping for the facilitated uptake of molecules. Processes. **9**, 913 (2021)
61. Lin, L., Dang, H., Zhu, R., Liu, Y., You, H.: Effects of side profile on acoustic streaming by oscillating microstructures in channel. Micromachines. **13**, 1439 (2022)
62. Lu, Y., Palanikumar, L., Choi, E.S., Huskens, J., Ryu, J., Wang, Y., Pang, W., Duan, X.: Hypersound-enhanced intracellular delivery of drug-loaded mesoporous silica nanoparticles in a non-endosomal pathway. ACS Appl. Mater. Interfaces **11**, 19734–19742 (2019)
63. Pan, S., Jeon, T., Luther, D.C., Duan, X., Rotello, V.M.: Cytosolic delivery of functional proteinsin vitro through tunable gigahertz acoustics. ACS Appl. Mater. Interfaces **12**, 15823–15829 (2020)
64. Zhang, Z., Wang, Y., Zhang, H., Tang, Z., Liu, W., Lu, Y., Wang, Z., Yang, H., Pang, W., Zhang, H., Zhang, D., Duan, X.: Hypersonic poration: a new versatile cell poration method to enhance cellular uptake using a piezoelectric nano-electromechanical device. Small **13**, 1602962 (2017)
65. Hashmi, A., Yu, G., Reilly-Collette, M., Heiman, G., Xu, J.: Oscillating bubbles: a versatile tool for lab on a chip applications. Lab Chip **12**, 4216 (2012)
66. Tang, Q., Liang, F., Huang, L., Zhao, P., Wang, W.: On-chip simultaneous rotation of large-scale cells by acoustically oscillating bubble array. Biomed. Microdevices **22**, 1–11 (2020)
67. Chowdhury, S.M., Abou-Elkacem, L., Lee, T., Dahl, J., Lutz, A.M.: Ultrasound and microbubble mediated therapeutic delivery: underlying mechanisms and future outlook. J. Control. Release **326**, 75–90 (2020)
68. Gao, Y., Wu, M., Lin, Y., Xu, J.: Trapping and control of bubbles in various microfluidic applications. Lab Chip **20**, 4512–4527 (2020)
69. Feng, J., Yuan, J., Cho, S.K.: Micropropulsion by an acoustic bubble for navigating microfluidic spaces. Lab Chip **15**, 1554–1562 (2015)
70. Li, Y., Liu, X., Huang, Q., Ohta, A.T., Arai, T.: Bubbles in microfluidics: an all-purpose tool for micromanipulation. Lab Chip **21**, 1016–1035 (2021)
71. Liu, J., Li, B., Zhu, T., Zhou, Y., Li, S., Guo, S., Li, T.: Tunable microfluidic standing air bubbles and its application in acoustic microstreaming. Biomicrofluidics **13**, 34114 (2019)
72. Gao, Y., Wu, M., Lin, Y., Zhao, W., Xu, J.: Acoustic bubble-based bidirectional micropump. Microfluid. Nanofluid. **24**, 1–10 (2020)
73. Zhang, W., Song, B., Bai, X., Jia, L., Song, L., Guo, J., Feng, L.: Versatile acoustic manipulation of micro-objects using mode-switchable oscillating bubbles: transportation, trapping, rotation, and revolution. Lab Chip **21**, 4760–4771 (2021)
74. Wang, A., Lin, I., Hsieh, Y., Shih, W., Wu, G.: Effective pressure and bubble generation in a microfluidic T-junction. Lab Chip **11**, 3499 (2011)
75. Ahmed, D., Ozcelik, A., Bojanala, N., Nama, N., Upadhyay, A., Chen, Y., Hanna-Rose, W., Huang, T.J.: Rotational manipulation of single cells and organisms using acoustic waves. Nat. Commun. **7**, 1–11 (2016)
76. Läubli, N.F., Gerlt, M.S., Wüthrich, A., Lewis, R.T.M., Shamsudhin, N., Kutay, U., Ahmed, D., Dual, J., Nelson, B.J.: Embedded microbubbles for acoustic manipulation of single cells and microfluidic applications. Anal. Chem. **93**, 9760–9770 (2021)
77. Tovar, A.R., Lee, A.P.: Lateral cavity acoustic transducer. Lab Chip **9**, 41–43 (2009)
78. Lieu, V.H., House, T.A., Schwartz, D.T.: Hydrodynamic tweezers: impact of design geometry on flow and microparticle trapping. Anal. Chem. **84**, 1963–1968 (2012)

79. Lu, X., Zhao, K., Peng, H., Li, H., Liu, W.: Local enhanced microstreaming for controllable high-speed acoustic rotary microsystems. Phys. Rev. Appl. **11**, 044064 (2019)
80. An, L.N., Deng, H., Devendran, C., Akhtar, N., Ma, X., Pouton, C., Chan, H.K., Neild, A., Alan, T.: Ultrafast star-shaped acoustic micromixer for high throughput nanoparticle synthesis. Lab Chip **20**, 582–591 (2020)
81. Rasouli, M.R., Tabrizian, M.: An ultra-rapid acoustic micromixer for synthesis of organic nanoparticles. Lab Chip **19**, 3316–3325 (2019)
82. Salari, A., Appak Baskoy, S., Ezzo, M., Hinz, B., Kolios, M.C., Tsai, S.S.H.: Dancing with the cells: acoustic microflows generated by oscillating cells. Small **16**, 1903788 (2019)
83. Mazalan, M., Noor, A., Wahab, Y., Yahud, S., Zaman, W.: Current development in interdigital transducer (IDT) surface acoustic wave devices for live cell in vitro studies: a review. Micromachines **13**, 30 (2022)
84. Frommelt, T., Kostur, M., Wenzel-Schäfer, M., Talkner, P., Hänggi, P., Wixforth, A.: Microfluidic mixing via acoustically driven chaotic advection. Phys. Rev. Lett. **100**, 34502 (2008)
85. Sun, C., Zhang, M., Huang, G., Zhang, P., Lin, R., Wang, X., You, H.: A microfluidic system of gene transfer by ultrasound. Micromachines **13**, 1126 (2022)
86. Thein, M., Cheng, A., Khanna, P., Zhang, C., Park, E., Ahmed, D., Goodrich, C.J., Asphahani, F., Wu, F., Smith, N.B., Dong, C., Jiang, X., Zhang, M., Xu, J.: Site-specific sonoporation of human melanoma cells at the cellular level using high lateral-resolution ultrasonic micro-transducer arrays. Biosens. Bioelectron. **27**, 25–33 (2011)
87. Ramesan, S., Rezk, A.R., Cevaal, P.M., Cortez-Jugo, C., Symons, J., Yeo, L.Y.: Acoustofection: high-frequency vibrational membrane permeabilization for intracellular siRNA delivery into nonadherent cells. ACS Appl. Bio Mater. **4**, 2781–2789 (2021)
88. Rezk, A.R., Ahmed, H., Ramesan, S., Yeo, L.Y.: High frequency sonoprocessing: a new field of cavitation-free acoustic materials synthesis, processing, and manipulation. Adv. Sci. **8**, 2001983 (2021)
89. Ozcelik, A., Rufo, J., Guo, F., Gu, Y., Li, P., Lata, J., Huang, T.J.: Acoustic tweezers for the life sciences. Nat. Methods **15**, 1021–1028 (2018)
90. Carugo, D., Ankrett, D.N., Glynne-Jones, P., Capretto, L., Boltryk, R.J., Zhang, X., Townsend, P.A., Hill, M.: Contrast agent-free sonoporation: the use of an ultrasonic standing wave microfluidic system for the delivery of pharmaceutical agents. Biomicrofluidics **5**, 44108 (2011)
91. Guo, X., Sun, M., Yang, Y., Xu, H., Liu, J., He, S., Wang, Y., Xu, L., Pang, W., Duan, X.: Controllable cell deformation using acoustic streaming for membrane permeability modulation. Adv. Sci. **8**, 2002489 (2021)
92. Lu, Y., de Vries, W.C., Overeem, N.J., Duan, X., Zhang, H., Zhang, H., Pang, W., Ravoo, B.J., Huskens, J.: Controlled and tunable loading and release of vesicles by using gigahertz acoustics. Angew. Chem. Int. Ed. Engl. **58**, 159–163 (2019)
93. Lu, Y., Huskens, J., Pang, W., Duan, X.: Hypersonic poration of supported lipid bilayers. Mater. Chem. Front. **3**, 782–790 (2019)
94. Wang, Z., Huang, P.H., Chen, C., Bachman, H., Zhao, S., Yang, S., Huang, T.J.: Cell lysis via acoustically oscillating sharp edges. Lab Chip **19**, 4021–4032 (2019)
95. Lu, X., Soto, F., Li, J., Li, T., Liang, Y., Wang, J.: Topographical manipulation of microparticles and cells with acoustic microstreaming. ACS Appl. Mater. Interfaces **9**, 38870–38876 (2017)
96. Zhou, Y., Ma, Z., Ai, Y.: Submicron particle concentration and patterning with ultralow frequency acoustic vibration. Anal. Chem. **92**, 12795–12800 (2020)
97. Song, B., Zhang, W., Bai, X., Feng, L., Zhang, D., Arai, F.: A novel portable cell sonoporation device based on open-source acoustofluidics. In: IEEE, pp. 2786–2791 (2020)
98. Grisanti, G., Caprini, D., Sinibaldi, G., Scognamiglio, C., Silvani, G., Peruzzi, G., Casciola, C.M.: A microfluidic platform for cavitation-enhanced drug delivery. Micromachines **12**, 658 (2021)
99. Goodwin, S.C., Bittner, C.A., Peterson, C.L., Wong, G.: Single-dose toxicity study of hepatic intra-arterial infusion of doxorubicin coupled to a novel magnetically targeted drug carrier. Toxicol. Sci. **60**, 177–183 (2001)
100. Li, Z.G., Liu, A.Q., Klaseboer, E., Zhang, J.B., Ohl, C.D.: Single cell membrane poration by bubble-induced microjets in a microfluidic chip. Lab Chip **13**, 1144–1150 (2013)
101. Marin, A., Massimiliano, R., Bhargav, R., Cheng, W., Sascha, H., Christian, J.K.: Three-dimensional phenomena in microbubble acoustic streaming. Phys. Rev. Appl. **3**, 041001 (2015)
102. Bourn, M.D., Batchelor, D.V.B., Ingram, N., McLaughlan, J.R., Coletta, P.L., Evans, S.D., Peyman, S.A.: High-throughput microfluidics for evaluating microbubble enhanced delivery of cancer therapeutics in spheroid cultures. J. Control. Release **326**, 13–24 (2020)
103. Carlo, D.D., Wu, L.Y., Lee, L.P.: Dynamic single cell culture array. Lab Chip **6**, 1445 (2006)
104. Centner, C.S., Murphy, E.M., Priddy, M.C., Moore, J.T., Janis, B.R., Menze, M.A., DeFilippis, A.P., Kopechek, J.A.: Ultrasound-induced molecular delivery to erythrocytes using a microfluidic system. Biomicrofluidics **14**, 24114 (2020)
105. Ankrett, D.N., Carugo, D., Lei, J., Glynne-Jones, P., Townsend, P.A., Zhang, X., Hill, M.: The effect of ultrasound-related stimuli on cell viability in microfluidic channels. J. Nanobiotechnol. **11**, 20 (2013)
106. Kim, R.: Advanced organotypic in vitro model systems for host–microbial coculture. BioChip J. **17**, 147–173 (2023)
107. Ahn, J., Sei, Y., Jeon, N., Kim, Y.: Tumor microenvironment on a chip: the progress and future perspective. Bioengineering **4**, 64 (2017)
108. Gupta, N., Liu, J.R., Patel, B., Solomon, D.E., Vaidya, B., Gupta, V.: Microfluidics-based 3D cell culture models: utility in novel drug discovery and delivery research. Bioeng. Transl. Med. **1**, 63–81 (2016)
109. Cai, Y., Fan, K., Lin, J., Ma, L., Li, F.: Advances in BBB on chip and application for studying reversible opening of blood–brain barrier by sonoporation. Micromachines **14**, 112 (2023)
110. Mobini, S., Song, Y.H., McCrary, M.W., Schmidt, C.E.: Advances in ex vivo models and lab-on-a-chip devices for neural tissue engineering. Biomaterials **198**, 146–166 (2019)
111. Chen, L., Raut, B., Nagai, N., Abe, T., Kaji, H.: Prototyping a versatile two-layer multi-channel microfluidic device for direct-contact cell-vessel co-culture. Micromachines **11**, 79 (2020)
112. Bagchi, S., Chhibber, T., Lahooti, B., Verma, A., Borse, V., Jayant, R.D.: In-vitro blood-brain barrier models for drug screening and permeation studies: an overview. Drug Des. Dev. Ther. **13**, 3591–3605 (2019)
113. Wang, J., Li, Z., Pan, M., Fiaz, M., Hao, Y., Yan, Y., Sun, L., Yan, F.: Ultrasound-mediated blood–brain barrier opening: an effective drug delivery system for theranostics of brain diseases. Adv. Drug Deliv. Rev. **190**, 114539 (2022)
114. Peruzzi, G., Sinibaldi, G., Silvani, G., Ruocco, G., Casciola, C.M.: Perspectives on cavitation enhanced endothelial layer permeability. Colloids Surf. B **168**, 83–93 (2018)
115. Deosarkar, S.P., Prabhakarpandian, B., Wang, B., Sheffield, J.B., Krynska, B., Kiani, M.F.: A novel dynamic neonatal blood-brain barrier on a chip. PLoS ONE **10**, e142725 (2015)

116. Bi, W., Cai, S., Lei, T., Wang, L.: Implementation of blood-brain barrier on microfluidic chip: recent advance and future prospects. Ageing Res. Rev. **87**, 101921 (2023)
117. Fan, Y., Xu, C., Deng, N., Gao, Z., Jiang, Z., Li, X., Zhou, Y., Pei, H., Li, L., Tang, B.: Understanding drug nanocarrier and blood–brain barrier interaction based on a microfluidic microphysiological model. Lab Chip **23**, 1935–1944 (2023)
118. Oh, H., Kang, M., Bae, E., Jung, Y., Cho, J., Poirier, J., Kim, J.S., Frampton, J.P., Choi, N., Chung, S.: Fabrication of hydrogel microchannels using aqueous two-phase printing for 3D blood brain barrier. BioChip J. **17**, 369–383 (2023)
119. Andreone, B.J., Chow, B.W., Tata, A., Lacoste, B., Ben-Zvi, A., Bullock, K., Deik, A.A., Ginty, D.D., Clish, C.B., Gu, C.: Blood-brain barrier permeability is regulated by lipid transport-dependent suppression of caveolae-mediated transcytosis. Neuron **94**, 581–594 (2017)
120. Juang, E.K., De Cock, I., Keravnou, C., Gallagher, M.K., Keller, S.B., Zheng, Y., Averkiou, M.: Engineered 3D microvascular networks for the study of ultrasound-microbubble-mediated drug delivery. Langmuir **35**, 10128–10138 (2019)
121. Park, Y.C., Zhang, C., Kim, S., Mohamedi, G., Beigie, C., Nagy, J.O., Holt, R.G., Cleveland, R.O., Jeon, N.L., Wong, J.Y.: Microvessels-on-a-chip to assess targeted ultrasound-assisted drug delivery. ACS Appl. Mater. Interfaces **8**, 31541–31549 (2016)
122. DeOre, B.J., Galie, P.A., Sehgal, C.M.: Fluid flow rate dictates the efficacy of low-intensity anti-vascular ultrasound therapy in a microfluidic model. Microcirculation **26**, e12576 (2019)
123. Driver, R., Mishra, S.: Organ-on-a-chip technology: an in-depth review of recent advancements and future of whole body-on-chip. BioChip J. **17**, 1–23 (2023)
124. Jang, M., Kim, H.N.: From single- to multi-organ-on-a-chip system for studying metabolic diseases. BioChip J. **17**, 133–146 (2023)
125. Zhang, B., Radisic, M.: Organ-on-a-chip devices advance to market. Lab Chip **17**, 2242–2395 (2017)
126. Cecen, B., Karavasili, C., Nazir, M., Bhusal, A., Dogan, E., Shahriyari, F., Tamburaci, S., Buyukoz, M., Kozaci, L.D., Miri, A.K.: Multi-organs-on-chips for testing small-molecule drugs: challenges and perspectives. Pharmaceutics **13**, 1657 (2021)
127. Tran, T.T.T., Delgado, A., Jeong, S.: Organ-on-a-chip: the future of therapeutic aptamer research? BioChip J. **15**, 109–122 (2021)
128. Ahn, J., Ko, J., Lee, S., Yu, J., Kim, Y., Jeon, N.L.: Microfluidics in nanoparticle drug delivery; from synthesis to pre-clinical screening. Adv. Drug Deliv. Rev. **128**, 29–53 (2018)
129. Beekers, I., van Rooij, T., Verweij, M.D., Versluis, M., de Jong, N., Trietsch, S.J., Kooiman, K.: Acoustic characterization of a vessel-on-a-chip microfluidic system for ultrasound-mediated drug delivery. IEEE Trans. Ultrason. Ferroelectr. Freq. Control **65**, 570–581 (2018)
130. Shi, J., Ma, Y., Zhu, J., Chen, Y., Sun, Y., Yao, Y., Yang, Z., Xie, J.: A review on electroporation-based intracellular delivery. Molecules **23**, 3044 (2018)
131. Wang, F., Lin, S., Yu, Z., Wang, Y., Zhang, D., Cao, C., Wang, Z., Cui, D., Chen, D.: Recent advances in microfluidic-based electroporation techniques for cell membranes. Lab Chip **22**, 2624–2646 (2022)
132. Tamosiunas, M., Mir, L.M., Chen, W.S., Lihachev, A., Venslauskas, M., Satkauskas, S.: Intracellular delivery of bleomycin by combined application of electroporation and sonoporation in vitro. J. Membr. Biol. **249**, 677–689 (2016)
133. Maciulevičius, M., Tamošiūnas, M., Jurkonis, R., Šatkauskas, S.: Dosimetric assessment of antitumor treatment by enhanced bleomycin delivery via electroporation and sonoporation. Bioelectrochemistry **146**, 108153 (2022)
134. Santra, T.S., Kar, S., Chang, H.Y., Tseng, F.G.: Nano-localized single-cell nano-electroporation. Lab Chip **20**, 4194–4204 (2020)
135. Zhang, Z., Zheng, T., Zhu, R.: Single-cell individualized electroporation with real-time impedance monitoring using a microelectrode array chip. Microsyst. Nanoeng. **6**, 81 (2020)
136. Zu, Y., Liu, X., Chang, A., Wang, S.: Flow micropillar array electroporation to enhance size specific transfection to a large population of cells. Bioelectrochemistry **132**, 107417 (2020)
137. Bhattacharjee, N., Horowitz, L.F., Folch, A.: Continuous-flow multi-pulse electroporation at low DC voltages by microfluidic flipping of the voltage space topology. Appl. Phys. Lett. **109**, 163702 (2016)
138. Luo, Y., Yobas, L.: Flow-through electroporation of mammalian cells in decoupled flow streams using microcapillaries. Biomicrofluidics **8**, 52101 (2014)
139. Wang, H., Lu, C.: Electroporation of mammalian cells in a microfluidic channel with geometric variation. Anal. Chem. **78**, 5158–5164 (2006)
140. Longsine-Parker, W., Wang, H., Koo, C., Kim, J., Kim, B., Jayaraman, A., Han, A.: Microfluidic electro-sonoporation: a multi-modal cell poration methodology through simultaneous application of electric field and ultrasonic wave. Lab Chip **13**, 2144–2152 (2013)
141. Adamo, A., Jensen, K.F.: Microfluidic based single cell microinjection. Lab Chip **8**, 1258 (2008)
142. Ghaemi, R., Arefi, P., Stosic, A., Acker, M., Raza, Q., Roger, J.J., Selvaganapathy, P.R.: A microfluidic microinjector for toxicological and developmental studies in Drosophila embryos. Lab Chip **17**, 3898–3908 (2017)
143. Gao, N., You, H.: Recent applications of point-of-care devices for glucose detection on the basis of stimuli-responsive volume phase transition of hydrogel. BioChip J. **15**, 23–41 (2021)
144. Fan, Q., Hu, W., Ohta, A.T.: Efficient single-cell poration by microsecond laser pulses. Lab Chip **15**, 581–588 (2015)
145. Yuan, F., Yang, C., Zhong, P.: Cell membrane deformation and bioeffects produced by tandem bubble-induced jetting flow. Proc. Natl. Acad. Sci. **112**, E7039–E7047 (2015)
146. Sharei, A., Zoldan, J., Adamo, A., Sim, W.Y., Cho, N., Jackson, E., Mao, S., Schneider, S., Han, M.J., Lytton-Jean, A., Basto, P.A., Jhunjhunwala, S., Lee, J., Heller, D.A., Kang, J.W., Hartoularos, G.C., Kim, K.S., Anderson, D.G., Langer, R., Jensen, K.F.: A vector-free microfluidic platform for intracellular delivery. Proc. Natl. Acad. Sci. **110**, 2082–2087 (2013)
147. Uvizl, A., Goswami, R., Gandhi, S.D., Augsburg, M., Buchholz, F., Guck, J., Mansfeld, J., Girardo, S.: Efficient and gentle delivery of molecules into cells with different elasticity via progressive mechanoporation. Lab Chip **21**, 2437–2452 (2021)
148. Alhmoud, H., Alkhaled, M., Kaynak, B.E., Hanay, M.S.: Leveraging the elastic deformability of polydimethylsiloxane microfluidic channels for efficient intracellular delivery. Lab Chip **23**, 714–726 (2023)
149. Dixon, A.J., Dhanaliwala, A.H., Chen, J.L., Hossack, J.A.: Enhanced intracellular delivery of a model drug using microbubbles produced by a microfluidic device. Ultrasound Med. Biol. **39**, 1267–1276 (2013)
150. Lee, S., Jeon, H., Shim, S., Im, M., Kim, J., Kim, J.H., Lee, B.C.: Preclinical study to improve microbubble-mediated drug delivery in cancer using an ultrasonic probe with an interchangeable acoustic lens. Sci. Rep. **11**, 1–10 (2021)
151. Rasouli, R., Paun, R.A., Tabrizian, M.: Sonoprinting nanoparticles on cellular spheroids via surface acoustic waves for enhanced nanotherapeutics delivery. Lab Chip **23**, 2091–2105 (2023)
152. Moore, R.P., O'Shaughnessy, E.C., Shi, Y., Nogueira, A.T., Heath, K.M., Hahn, K.M., Legant, W.R.: a multi-functional

microfluidic device compatible with widefield and light sheet microscopy. Lab Chip **22**, 136–147 (2021)
153. Prajapati, E., Kumar, S., Kumar, S.: Muscope: a miniature on-chip lensless microscope. Lab Chip **21**, 4357–4363 (2021)
154. Rong, N., Zhou, H., Liu, R., Wang, Y., Fan, Z.: Ultrasound and microbubble mediated plasmid DNA uptake: a fast, global and multi-mechanisms involved process. J. Control. Release **273**, 40–50 (2018)
155. Bansal, K., Jha, C.K., Bhatia, D., Shekhar, H.: Ultrasound-enabled therapeutic delivery and regenerative medicine: physical and biological perspectives. ACS Biomater. Sci. Eng. **7**, 4371–4387 (2021)
156. Au, A.K., Huynh, W., Horowitz, L.F., Folch, A.: Mikrofluidik aus dem 3D-Drucker. Angew. Chem. **128**, 3926–3946 (2016)
157. Liu, C., Wan, T., Wang, H., Zhang, S., Ping, Y., Cheng, Y.: A boronic acid-rich dendrimer with robust and unprecedented efficiency for cytosolic protein delivery and CRISPR-Cas9 gene editing. Sci. Adv. **5**, eaaw8922 (2019)
158. Sharei, A., Poceviciute, R., Jackson, E.L., Cho, N., Mao, S., Hartoularos, G.C., Jang, D.Y., Jhunjhunwala, S., Eyerman, A., Schoettle, T., Langer, R., Jensen, K.F.: Plasma membrane recovery kinetics of a microfluidic intracellular delivery platform. Integr. Biol. (Camb.) **6**, 470–475 (2014)
159. Bhatia, S.N., Ingber, D.E.: Microfluidic organs-on-chips. Nat. Biotechnol. **32**, 760–772 (2014)
160. Amoyav, B., Goldstein, Y., Steinberg, E., Benny, O.: 3D printed microfluidic devices for drug release assays. Pharmaceutics **13**, 13 (2021)